CHALMERS

A 5 MW Wind Turbine Generator System for a DC grid application

Master of Science Thesis

ARASH MAZAHERI

Department of Energy and Environment *Division of Electric Power Engineering*
CHALMERS UNIVERSITY OF TECHNOLOGY
Göteborg, Sweden 2012

A 5 MW Wind Turbine Generator System for a DC grid application

Arash Mazaheri

Department of Energy and Environment
Division of Electric Power Engineering
CHALMERS UNIVERSITY OF TECHNOLOGY
Göteborg, Sweden 2012

A 5 MW Wind Turbine Generator System for a DC grid application
ARASH MAZAHERI

Department of Energy and Environment
Division of Electric Power Engineering
Chalmers University of Technology
SE–412 96 Göteborg
Sweden
Telephone +46 (0)31–772 1000

Cover:
Text concerning the cover illustration. In this case: Wind turbine tower taken by the author.

Chalmers Bibliotek, Reproservice
Göteborg, Sweden 2012

Diode Rectifier and DC/DC-Converter for 5 MW Wind Turbine Generator System and DC Collection Grid

Arash Mazaheri

Department of Energy and Environment Division of Electric Power Engineering Chalmers University of Technology

Abstract

- In this work a robust generating system for a 5 MW PMSM wind turbine system with diode rectifier and DC/DC converter connected to DC link has been investigated. The design and efficiency have been studied using MATLAB Simulink and SIMPLORER and the result shows that this system topology has high efficiency.
- The result found was that the same generator that can provide 5 MW using an IGBT-Converter, can only give 2.5 MW using a diode rectifier and a variable DC-link. However, with series and parallel compensations the same generator can provide an output power even more than 5 MW. It was also found that the efficiencies of systems at rated operation with IGBT-converter, diode rectifier with series compensation and shunt compensation are 97.6%, 98.6%, and 98.9%, respectively. Moreover, the systems efficiency at 5% of load are 93.0%, IGBT-converter, 97.3%, series compensation, and 95.3%, shunt compensation.
- The required reactive power for series compensation and shunt compensation to provide 5 MW output power for the diode rectifier system, at rated operation, are 1.5 MVar and 2.8 MVar, respectively.
- To conclude, the diode rectifier with series compensation is more efficient for low wind speed (4-11m/s) also it needs less reactive power; however, the shunt compensation scenario has better efficiency at rated speed when the wind speed is higher than 12m/s.

Index Terms: Diode rectifier, DC/DC converter, PMSM, wind power generator, synchronous generator, DC collection, HVDC.

Acknowledgements

This work has been carried out at the Department of Energy and Environment at Chalmers University of Technology. Facilities provided by the Department during the Master thesis work are gratefully acknowledged.

Even though only my name appears on the cover of this thesis report, great many people have contributed to its production. I owe my gratitude to all those people who have made this dissertation possible.

It gives me great pleasure in acknowledging the support and help of Professor Torbjörn Thiringer for his supervision, patience and giving me the opportunity to work on this project.

One of the most interesting parts of this project has been the time that I spent with dear Poopak Roshanfekr Fard to solve the problems and investigate the behaviour of the system. I would like to thank dear Poopak for her friendship, continuous help and excellent support.

I wish to express my love and gratitude to my beloved extended family, for their understanding, support and endless love. I would like to express my heart-felt gratitude to my mom, Azin, Mana, and Gelareh.

Most importantly, none of this would have been possible without the love and patience of my love, dear Afsaneh.

Arash Mazaheri
Göteborg, Sweden, 2012

Contents

Table of Contents

Abstract ..... **iii**
Acknowledgements ..... **v**
Table of Contents ..... **vii**
1. Introduction **1**
1.1 Problem background 1
1.2 Previous work 2
1.3 Purpose 2
2. Theory **3**
2.1 Synchronous Generators 3
2.1.1 Electrically magnetized synchronous generator 3
2.1.2 Permanent Magnet Synchronous Generator 4
2.2 Wind turbine and wind energy 5
2.3 Diode rectifier 6
2.3.1 Diode Characteristics 6
2.4 Full bride DC/DC converter 10
2.5 Loss calculation 11
2.5.1 Diode loss Calculation 11
2.5.2 IGBT-converter loss calculation 12
2.5.3 Generator loss calculation 13
3. Case set-up **14**
3.1 System Topology 14
3.2 Aerodynamic Conversion 14
3.3 Permanent Magnet Synchronous Generator 16
3.3.1 Verification of the dynamic model 17
3.4 Three-phase full bridge diode rectifier 23

3.5 Measurement modules 24
3.5.1 Three-Phase V-I and P-Q Measurement Blocks 25
3.5.2 RMS method 25
3.5.3 Instantaneous power measurement 26
4. Analysis Part 28
4.1 Simulations 28
4.1.1 Diode rectifier connected to voltage stiff 28
4.1.2 Operation of a Diode-rectifier in DCM 30
4.1.3 Operation of Diode-rectifier in CCM 32
4.2 Power transmission 43
4.2.1 Series compensation 44
4.2.2 Shunt compensation 46
4.2.3 Effect of core saturation 48
4.3 Loss determination 49
4.3.1 Diode losses 49
4.3.2 IGBT-converter losses 51
4.3.3 Generator losses 51
4.4 Equilibrium DC voltage and losses 55
4.5 Diode rectifier vs. active rectifier 59
5. Conclusions 65
5.1 Results from present work 65
5.2 Future work 66
References 67
Appendix 69

Chapter 1

1. Introduction

1.1 Problem background

Wind speed plays the most important role in wind power generation since the energy in the wind is proportional to the cube of the wind speed. In a windy region the average wind speed during a year is about 9.4m/s. Therefore, if the mean speed is lowered to 6m/s instead of 6.5m/s the available power decreases by 21%. The average wind speed is higher offshore [1], also the visual and noise impact of wind farms are mitigated within the sea, which makes sea based installations attractive. In addition, there is an upcoming shortage of space on land for wind energy installation. Hence, an important certain future scenario of wind energy is as offshore wind farms, which demands robust, highly efficient, economical designs and constructions.

In spite of the fact that higher wind speed, less turbulence, lower wind shear and possibility to have bigger wind farms are advantages of offshore construction, more expensive installation, construction and maintenance are the drawbacks. It is crucial to find a way to decrease the cost of electricity generation to make it more interesting for both suppliers and consumers. Remote-located wind parks with very long transmission lines need an effective transmission path to transfer energy from offshore to consumers, so HVDC is more highlighted and instead of having huge offshore platforms for HVDC equipment, high frequency dc/dc converters can be attached to small platforms attached to the wind turbines. Due to robustness and low needed maintenance, synchronous generators have been taking an important role in offshore wind farms. One of the advantaged of using DC/DC converter is a possibility for elimination of huge construction for large transformers [2].

As was mentioned, construction of large offshore wind farms are attractive due to the limitation of available places for wind turbines on land, and together with the fact that the HVDC might be used, it would obviously be of high interest to produce a DC-output from the generator system instead of 50 Hz AC as usual. Therefore, there is a need to study large wind turbines with high power output (in our case 5MW) as well as high rectified voltage to transmit power from long distances with low power losses.

1.2 Previous work

This thesis work is a part of a bigger project which is designing the whole system for wind farms. The concept of the primary project is to design a wind farm using HVDC for the collection grid which includes designing generators, high frequency transformers, diode/IGBT rectifiers, and DC/DC converters. The aim is to boost up the outputs of the investigating generating system to 200 kV DC voltage. First the AC voltage should be rectified, and then in two stages it will be reached to 200kV. In a previous Master Thesis [2], a basic and robust system for wind turbine system connected to a DC link has been investigated. The boundaries of the thesis are from Synchronous generator output to about 5-10kV DC.

1.3 Purpose

The purpose of this thesis is to design a diode rectifier for a 5 MW PMSM. Moreover, to determine the efficiency of the system as well as the possible power extraction that can be made from the generator. To utilize series and shunt compensation is furthermore of high importance. Finally, a study shall be carried out to estimate which are the key factors for making this system successful, then the losses of this system shall be compared with those obtained using an active rectifier. However, to do the final economical evaluation of the IGBT versus diode system is not a purpose; instead it will be left for further work.

Chapter 2
2. Theory

2.1 Synchronous Generators

Synchronous generators are using permanent magnet or electrical excitation to provide the excitation field. Commonly, to convert the output mechanical power of hydro, steam and gas turbines, reciprocating engines and wind turbines into electrical power, these kinds of generators are used in constant speed operation when the speed of rotor always matches the supply frequency (50, 60Hz) with some multiple. This multiple can be solved using a gearbox and by adjusting the pole number of the machine. However, thanks to power electronic converters, a power control is facilitated and these machines can accordingly be used in variable speed applications. In this case, the output voltage and frequency can be made to vary with wind speed. Fig. 2.1 shows a typical set-up of a wind turbine with a gearbox.

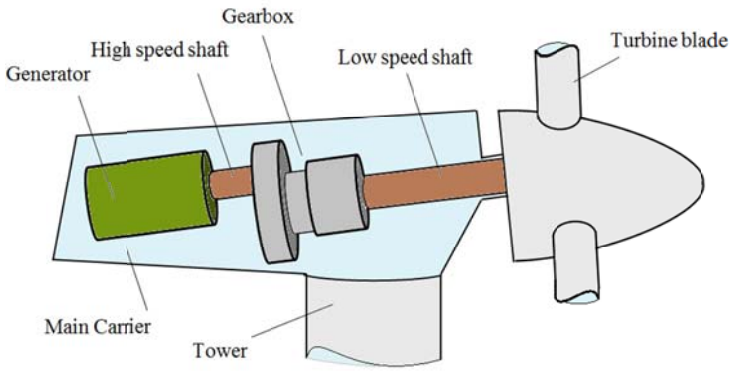

Fig. 2.1 Wind turbine scheme

2.1.1 Electrically magnetized synchronous generator

In this type of generator the DC flux is generated by a DC current in the rotor, provided either through slip-rings or with a brushless exciter with a rotating rectifier. Then the rotor is driven by a turbine with a certain speed; consequently the rotating field flux induces a voltage in the stator winding and the speed of the synchronous generator is obtained according to the number of poles and the frequency.

The EMSG is mainly used in hydroelectric and thermoelectric plants. However, some investments have been put to utilize the EMSG in wind farms. For instance, ENERCON is producing a gearless wind generator design with a low-speed synchronous generator [3].

2.1.2 Permanent Magnet Synchronous Generator

The fact that the use of the PMSG has increased, is that the PMSG has some advantages which make it more desirable to be used in wind turbines.

First, the magnetic field is provided by the permanent magnet and there is no need for additional DC supply for magnetization (excitation circuit). Therefore, without slip rings, and brushes the machine becomes more robust and maintenance free.

Second, the efficiency of the PMSG in comparison with EMSG is higher. Since, the rotor copper losses disappear as there is no rotor winding.

The Permanent Magnet Synchronous Machine as a wind generator operates in the generator mode. The mode of operation is dictated by the mechanical torque (wind energy). By using a second-order state-space model, the electrical and mechanical parts of the generator can be represented.

In a dq-model the windings are assumed to be sinusoidally distributed and producing a flux from the permanent magnets so that they produce three-phase back EMF waveforms. The dq-model using amplitude invariant transformation of the PMSG is represented by

$$\frac{d}{dt}i_d = \frac{1}{L_d}v_d - \frac{R}{L_d}i_d + \frac{L_q}{L_d}p\omega_r i_q$$

$$\frac{d}{dt}i_b = \frac{1}{L_q}v_q - \frac{R}{L_q}i_q - \frac{L_d}{L_q}p\omega_r i_d - \frac{\psi p\omega_r}{L_q} \tag{2-1}$$

$$T_e = 1.5p\left(\psi . i_q + (L_d - L_q)i_d i_q\right).$$

Here R is the resistance of the stator windings and accordingly L_d, L_q, v_d, v_q, I_d, and I_q are inductances, voltages and currents on d and q axis. ω_r, ψ, p, T_e are the angular velocity of the rotor, amplitude of the flux induced by the permanent magnets of the rotor in the stator, number of pole pairs and electromagnetic torque, respectively [4].

The L_q and L_d inductances symbolize the relation between the phase inductance and

the rotor position due to the saliency of the rotor. For example, the inductance measured between phase *a* and *b* (phase c is left open) is given by

$$L_{ab} = L_d + L_q + \left(L_q - L_d\right)\cos(2\theta + \frac{\pi}{3})$$

where θ represents the electrical angle [4].

These equations are expressed in the phase reference frame (dq frame). Note that L_q and L_d inductances represent the relation between the phase inductance and the rotor position due to the saliency of the rotor. For a non-salient rotor L_q and L_d becomes equal and the measured inductance is the projection of inductances on *d* and *q* axis.

2.2 Wind turbine and wind energy

In order to reduce mechanical stress, and have less audible noise as well as better power quality, variable speed wind turbines are designed to operate over a range of wind speeds. A typical wind turbine rotor has a speed of 10-20 rpm and a normal generator with low pole number operates with a speed of 1000-1500 rpm. The useful conversion of wind energy to rotor speed is much lower than the needed speed for rotating a generator with low pole number [5].

$$n_s = \frac{120\,f}{P_{number\ of\ poles}} \tag{2-2}$$

The relation between produced power and wind speed is

$$P_{mech} = \frac{1}{2}\rho_{air} A_r C_p \omega_w^3 \tag{2-3}$$

where ρ_{air}, C_p, A_r, and ω_w are the air density, the power coefficient, the area swept by rotor, and the wind speed. P_{mech} is the mechanical energy on the shaft of the turbine which can be extracted from the energy in the wind. C_p is a function of the tip speed ratio when ω_r is the rotor speed. λ is tip speed ration and can be found as

$$\lambda = \frac{\omega_r}{\omega_w} \tag{2-4}$$

Considering the cubic relationship of wind speed and mechanical power, a gearbox can be used to adjust the wind turbine rotor speed to the generator speed; however synchronous generators with high number of poles can either eliminate the need of high speed rotation or reduce the size and number of stages of a gearbox. The tip speed ratio

is also an important parameter; as it is shown, the mechanical power is a function of the tip speed ratio. Thus, the rotor speed should be adjusted in order to achieve the maximum mechanical power at every wind speed. It is important to operate the wind turbine according to an optimal value of the tip speed ratio.

2.3 Diode rectifier

Technology development and the cost decrease of power electronic devices make power converters be more common. The first conversion of AC output voltage of a generator to a DC voltage could be the duty of a diode rectifier. Since this kind of rectifier is inexpensive and robust, a diode rectifier can be an interesting option where power can flow from AC side to DC side [6].

2.3.1 Diode Characteristics

A diode which is shown in Fig. 2.2 is a semiconductor made of Silicon, Germanium, Silicon Carbide or Selenium. The important property of a diode is its directional conduction which means that it conducts electric current in one direction, form anode to cathode. When the anode is positively charged relative to the cathode and an applied voltage over the diode is greater than a definite forward threshold voltage, the diode starts to conduct and the current flows from anode to cathode. If the diode is reversed biased or the voltage across the diode is less than forward threshold voltage, then the diode blocks the current. The steady state *i-v* characteristic of the diode is shown in Fig. 2.3

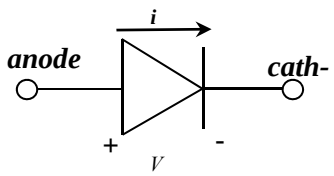

Fig. 2.2 diode symbol

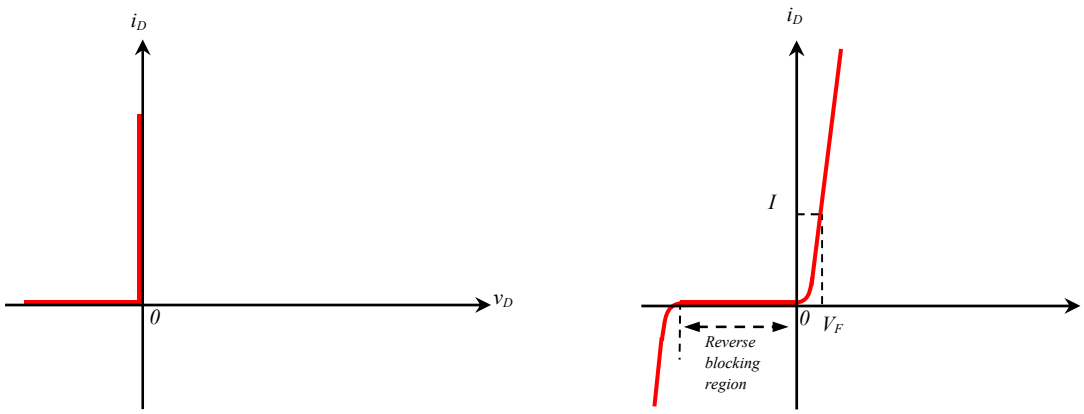

Fig. 2.3 i-v characteristic of a diode, left-hand is the idealized and right-hand is the actual

It is seen that the diode in its forward biased region start to conduct with a small forward threshold voltage; this voltage drop over the diode is about 1 V. In normal operation the diode works either in the reverse blocking region or in the forward biased region which is the conduction region. By neglecting the voltage drop over the diode, the ideal *i-v* characteristic curve is obtained and then the diode acts like a switch.

Fig. 2.4 shows that the diode lets a negative current flow during the reverse recovery time. The diode current reverses for a specific time at turn-off. The extra carriers sweep out which makes a negative current flowing in the diode. Then the diode can block a negative voltage. In other words, the reverse recovery time is the needed time for the electrons to get back to the n-region and for the holes to be swept out to recombination in the p-region; then the free carriers flowing across the junction are extinguished and the diode blocks the negative current, Fig. 2.5. The charge flowing during reverse recovery time is reverse recovery charge which is represented by Q.

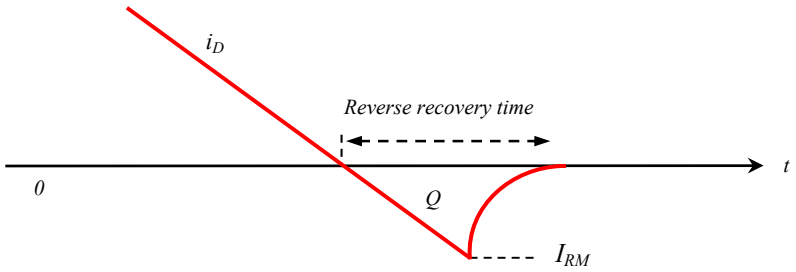

Fig. 2.4 Reverse recovery

The idealized characteristic can be used for analyzing the system, but for the calculation of the losses and also for the design of the system, the actual curve should be considered. Different types of diodes are available based on the application requirements.

- Line-frequency diodes.

  These diodes are designed to have an on-state voltage as low as possible; consequently they have larger reverse recovery time which is acceptable for line-frequency applications. The blocking voltage rating of these diodes could be several thousand volts with several thousand amperes as forward conductions ability. They can also be connected in series and parallel for different voltage and current requirements.

  As the ideal diode was discussed, the cross sectional view of a pn-junction power diode, the practical realization, is shown in Fig. 2.5.

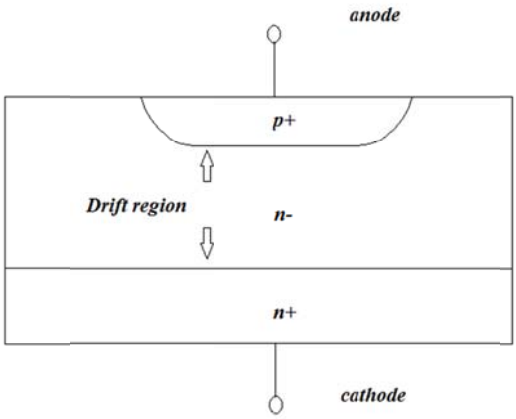

Fig. 2.5 Cross sectional view of a power diode

For the diode in power application, the n-type layer is heavily doped and a light doped n^- crystal layer is grown on it. Afterwards, a heavily doped p-type region, which makes the anode to be diffused in, which forms the *pn* junction [6].

The reverse breakdown voltage of a diode depends on the thickness of the drift region. The n^- -type layer (drift region), which absorbs the depletion layer of the reverse biased junction, distinguishes power diodes from low power diodes. This layer could be relatively thick or more than average width for large reverse voltages which results in a high Ohmic resistance when the diode is forward biased. High voltage and large current with considering high Ohmic resistance can lead to excessive power dissipation when it is conducting current. However, by taking into account some mechanisms; this problem

can be reduced [6].

Although, at a large current, the dissipation in the drift region of a power diode should not be ignored, since these losses limit the final power capability, the resistance of the drift region decreases because of the huge amount of excess-carrier injection into the resistance of the drift region. At high injection level, since the hole space is very large, the hole space can attract electrons from the n^+ region into the drift region. This takes electrons from both the n^- and n^+ region into the drift region with equal densities. The diffusion of holes and injection of electrons lead to recombination into the drift region which is called double injection. This results in an increase of carrier distribution in the drift region when the diffusion length is greater than the drift region. Therefore, the drift region conductivity becomes higher [6].

In order to make the voltage drop across the drift region lower, the diffusion length should be well-matched with the drift region length. This can reduce the dissipation losses with the same current density.

- Schottky diodes.

  These diodes have a low forward voltage drop in very low output voltage circuit, 50 to 100 V. The structure of Schottky diode is a thin metal film, usually placed on n-type semiconductor, in direct contact with a semiconductor, as shown in Fig. 2.6.

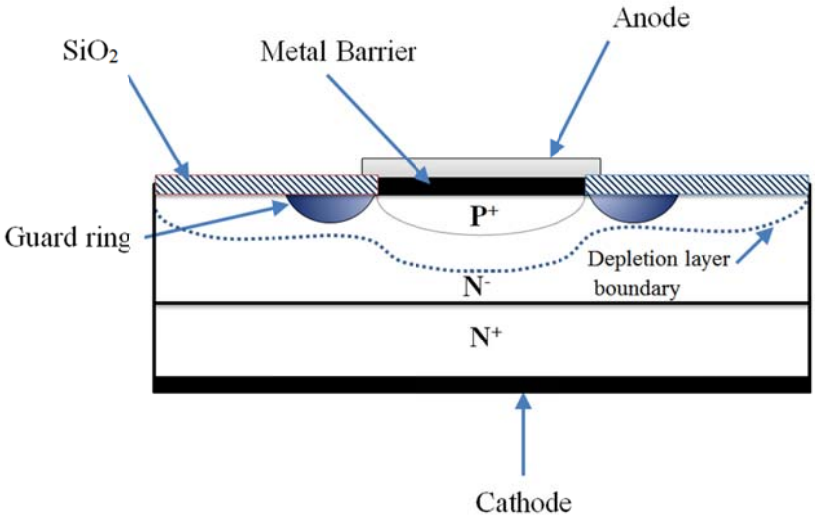

Fig. 2.6 Cross sectional view of a Schottky diode

The metal film, anode, can be Aluminum and the cathode is the semiconductor. As it was mentioned, Schottky diodes have a significantly low on-state voltage, 0.3-0.4 V. However, they have high reverse current in comparison with a silicon *pn*-junction

diode.

- Fast recovery diodes.

  These diodes are designed to operate in high-frequency applications where a small recovery time is required. These kinds of diodes have reverse recovery time of less than a few microseconds for several hundred volts and amperes output. Although fast diodes are optimized for fast transmission from conducting to blocking state, they have higher conduction losses compered to line-frequency diodes. They can be used as a complementary diode for IGBTs, GTOs, or IGCTs [7]. Reducing the reverse recovery time has a bad effect on the on-state losses, due to the increase of forward drop voltage. However, to obtain the optimal dynamic behaviour for high dynamic changes in both voltage and current, the efficiency of doping profile (the emitter) and carrier lifetime in high and a low doped region should be optimised.

2.4 Full bride DC/DC converter

A full bridge converter is a dc-dc converter where the output voltage and current of the converter can be controlled and this ability provides it to work in all four quadrant of the i_o-v_o plane, therefore the power flow of the converter can be either positive or negative [6]. However, by having a diode rectifier before the converter, it is not possible to have a negative current.

The input of the full bridge converter is the DC voltage formed by a diode rectifier. Then the full bridge provides a high frequency voltage square wave for the input of high frequency transformer. The full bridge converter can be controlled in two different ways:

- Duty cycle control
- Phase shift control

Since, the output voltage of the converter is proportional to the duty cycle, controlling the full bridge by altering the duty cycle can be the first option. However switching losses are high when using this method [8]. In phase shift control, the two switching legs can be controlled independently which gives lower switching losses. The responsibility of the leading leg is to change the converter to active phase and the lagging leg changes the converter to passive phase.

Fig. 2.7 shows a full bridge converter which has two legs and each leg has two switches and two diodes.

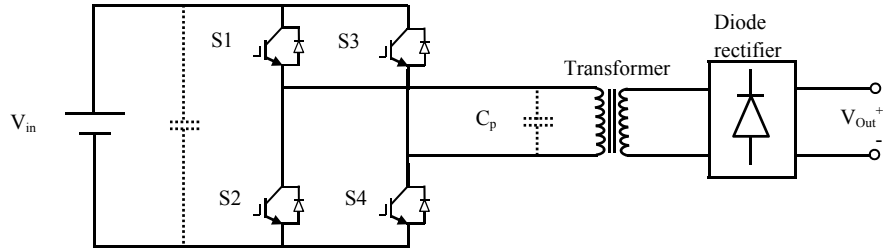

Fig. 2.7 Full bridge converter

2.5 Loss calculation

In this thesis, the focus of the loss determination will be on the comparison of the diode rectifier and the IGBT-converter. The diode loss calculation and the losses in IGBT model will be presented in this part. In addition to the semiconductor losses, the losses in the generator should also be determined.

2.5.1 Diode loss Calculation

The diode losses involve both static and dynamic losses where the static losses are conducting losses and dynamic losses are referred to as switching losses.

The conduction loss of a diode can be expressed as function of forward drop voltage versus current. Since the leakage current in the *pn*-junction diodes is very low, it can be neglected. The static dissipation losses can be calculated by

$$P_{static} = \frac{1}{T}\int v_{diode} i_{diode} \tag{2-5}$$

For the dynamic losses, the turn-off losses are dominant compared to turn-on losses. Thus, the switching losses of a *pn*-junction diode is almost practically the same as turn-off losses which depends on the reverse-recovery time of the diode when the state of diode is changing from conduction to blocking state. The charge stored during the forward conduction in the diode produces the energy dissipation during transition from conduction to turned-off condition. When a reverse voltage is applied to the diode, the stored charge in the diode should be removed by a reverse current [9]. Then a negative current spike occurs in the diode while the diode is still forward biased which results in dynamic losses. As it is shown in [10] the switching losses of a pn-junction diode can be calculated as

$$P_{sw} = J_f \tau_a V_f f_s \tag{2-6}$$

where J_f, τ_a, V_f, f_s are current density (A/cm^2), ambipolar carrier life time (s), forward operating voltage (V), and switching frequency respectively. The recent equation can be expressed as E_r which is reverse recovery energy multiply with switching frequency. E_r is related to operation voltage, *di/dt*, temperature and stray inductances. Fig. 2.8 shows the current, voltage wave forms and corresponding switching losses.

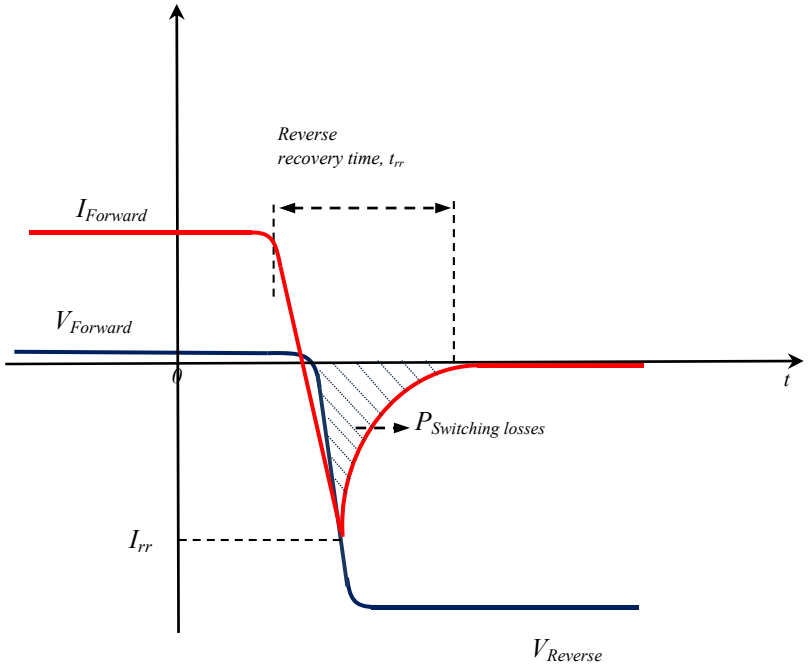

Fig. 2.8 Current and voltage of diode in switching

2.5.2 IGBT-converter loss calculation

The most dominant losses in the IGBT-converter, in its steady-state operation, are conduction and switching losses. The other losses such as gate driver losses, auxiliary circuit losses, capacitor losses and snubber losses are not considered in this work. It is assumed that there is sufficient heat transfer for the converter to operate at the rating temperature. The equations originating from [11] have been used in order to calculate the losses in the IGBT-converter [12].

$$P_{cond\_IGBT} = \left(\frac{1}{2\pi} + \frac{M\cos\varphi}{8}\right) V_{CE0}\hat{I}_1 + \left(\frac{1}{8} + \frac{M\cos\varphi}{3\pi}\right) r_{CE}.\hat{I}_1^2 \quad (2\text{-}7)$$

$$P_{cond\_D} = \left(\frac{1}{2\pi} - \frac{M\cos\varphi}{8}\right) V_{F0}\hat{I}_1 + \left(\frac{1}{8} - \frac{M\cos\varphi}{3\pi}\right) r_F.\hat{I}_1^2 \quad (2\text{-}8)$$

where P_{cond_IGBT} and P_{cond_D} are the conduction losses in the IGBT and diode, respectively. M is the modulation index, $\cos\varphi$ is the power factor, $\hat{I}_1$ is the peak value of the stator current, V_{CE0} is the voltage of the IGBT and V_{F0} is the voltage of the diode at the very low current.

$$P_{sw\_D} = f_{sw}E_{sw\_D}\left(\frac{1}{\pi}.\frac{\hat{I}_1}{I_{ref}}\right)^{K_i}.\left(\frac{V_{CC}}{V_{ref}}\right)^{K_v} \quad (2\text{-}9)$$

$$P_{sw\_IGBT} = f_{sw}E_{sw}\left(\frac{1}{\pi}.\frac{\hat{I}_1}{I_{ref}}\right)^{K_i}.\left(\frac{V_{CC}}{V_{ref}}\right)^{K_v} \quad (2\text{-}10)$$

$$E_{sw} = E_{sw_{IGBT_{on}}} + E_{sw\_IGBT\_off} \quad (2\text{-}11)$$

P_{sw_D} and P_{sw_IGBT} are the switching losses for the diode and the IGBT, respectively. f_{sw} is the switching frequency, V_{CC} is the voltage of the module, I_{ref} is the IGBT current level and V_{ref} is the module reference voltage at which the switching losses are given. E_{sw} and E_{sw_D} are the switching energy loss for the transistor and the diode at I_{ref} and V_{ref}. r_{CE} and r_F are the semiconductor resistances. The scaling factors K_i and K_v are 0.6 for the diode while they are 1 and 1.35 for the IGBT [12].

2.5.3 Generator loss calculation

Main generator losses consist of iron and copper losses and other loss components in the machine have not been considered. The Iron loss is relative to speed squared as

$$P_{Fe} = k\omega_{el}^2 \quad (2\text{-}12)$$

where P_{Fe} is the iron loss, k is 0.101 and ω_{el} is the machine electrical speed in *rad/s* [12]. The copper loss of the machine is the Ohmic losses in the stator and can be obtained by

$$P_{copp} = 3RI^2 \quad (2\text{-}13)$$

where R is the stator phase resistance and I is the RMS phase current.

Chapter 3

3. Case set-up

In this section, first the system topology and components used in this thesis will be studied, and then the next chapter will show the simulation and the results of this topology.

3.1 System Topology

There are different ways to convert the mechanical power from the rotor blades to electrical energy. The here suggested wind turbine system is depicted in Fig. 3.1 which consists of a three phase diode rectifier and an ideal full bridge DC/DC converter with current control for a 5 MW PMSM.

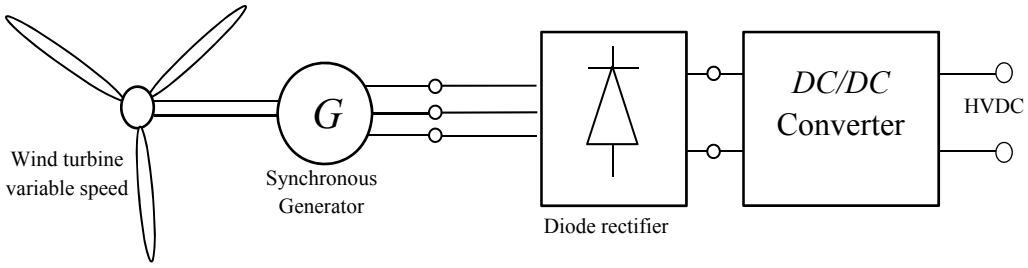

Fig. 3.1 System topology

Even though the output voltage of a diode rectifier can vary with the rotor speed, the dc-output voltage is set by the DC/DC converter.

3.2 Aerodynamic Conversion

A part of the available power in the wind is converted to mechanical power. The amount of energy converted from energy in the wind to mechanical energy as was discussed is related to C_p. In the C_p-λ curve, C_p is a function of tip speed ratio, Fig. 3.2. Since the maximum mechanical power is desirable to be extracted from the energy in the wind, the maximum C_p is used for the wind speed from 3 m/s to 12 m/s;

however when the wind speed becomes higher than 12 m/s, the power should be limited then C_p decreases. The decrease of C_p is become possible by changing the pitch angle.

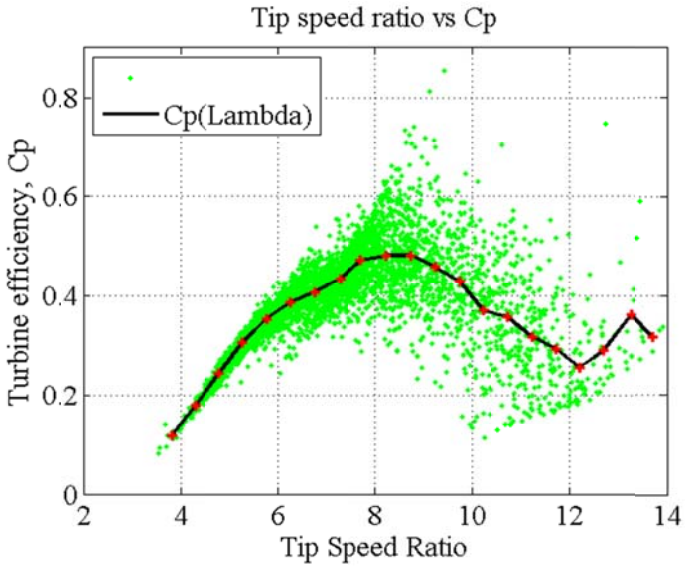

Fig. 3.2 C_p-λ curve

Therefore, there is a linear relationship between the rotor speed and the wind speed from 3 m/s up to 8 m/s, see Fig. 3.3. When the wind speed reaches 10 m/s, the rotor speed is kept constant and the input speed for the PMSG becomes 750 RPM. The data used in the simulation is taken from [13].

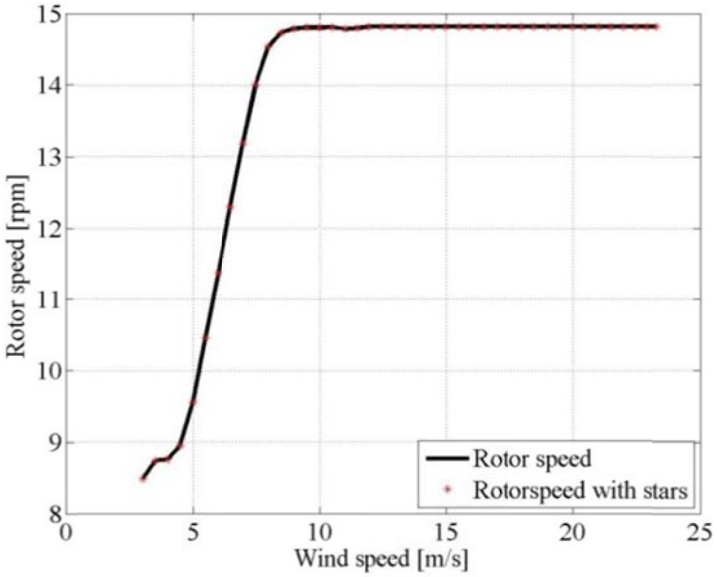

Fig. 3.3 Rotor speed- wind speed

3.3 Permanent Magnet Synchronous Generator

As was mentioned before, a dynamic model of three-phase PMSG has been used. The sinusoidal model assumes that the flux established by the permanent magnets in the stator is sinusoidal, which implies that the electromotive forces are sinusoidal.

In this work a PMSG designed for the rated output power of 5 MW has been studied. The data of the investigating generating system is provided in the appendix. However the main required data for the simulation is shown in Table 3-1.

Table 3-1 PMSG data

Parameters	Value	Unit
Rated Output Power	5000	kW
Rated Voltage	4800	V
Stator phase resistance R_s	0.0374772	Ohm
Stator phase inductance L_s	15.3725	mH
Fundamental Induced RMS Line Voltage	5032	V
Flux linkage established by magnets	16.026	Vs
Number of poles	4	
Back EMF waveform	Sinusoidal	

Fig. 2.1 Shows that how the power output of a wind turbine varies with wind speed [13].

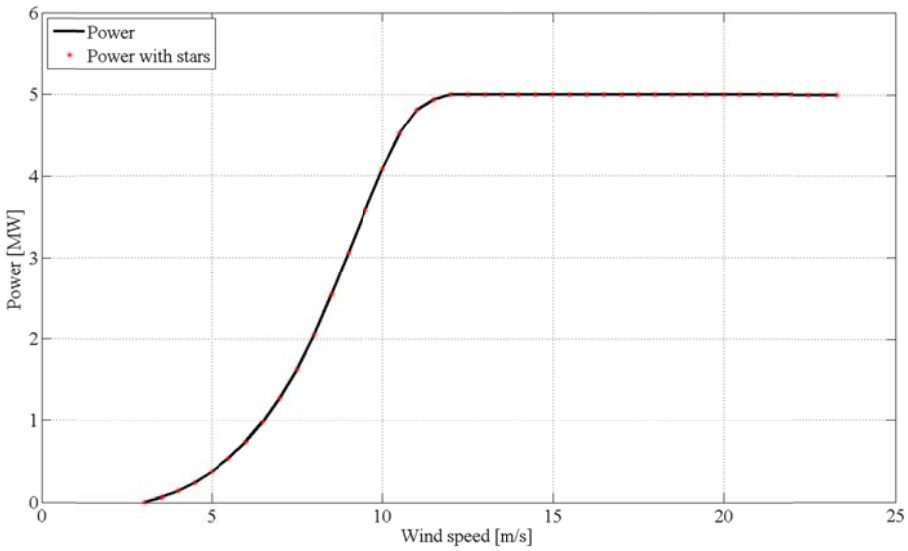

Fig. 3.4 Output power of wind turbine for different wind speeds

3.3.1 Verification of the dynamic model

The dynamic model of the permanent magnet generator must work properly according to the designed model [12]. In order to analyse the system behaviour, it is necessary to obtain the line to ground voltage, and phase-currents. Then the output power of the generator and losses can be calculated and investigated.

At no-load operation the fundamental induced RMS line voltage in the generator is 5032 [V] which is established by the magnets' flux linkage. Therefore the flux linkage for no-load operation is

$$\psi_m = \frac{\frac{V_{RMS}\sqrt{2}}{\sqrt{3}}}{\omega_e} = 13.08 \text{ [Vs]}. \tag{3-1}$$

The power angle of the PMSG, the angle between the induced voltage and current, is 80°. Therefore, at full load operation the current is

$$i = \frac{E\angle -80^\circ - V\angle 0^\circ}{jX} = \frac{4108\angle -80^\circ - 4000\angle 0^\circ}{j4.8} = 1080\angle -39^\circ \tag{3-2}$$

The RMS phase current is 763.67 [A] and RMS phase voltage is 2828.4 [V]. The power factor is 0.776 and the transferred power becomes 5 [MW]. In order to investigate the PMSG two models have been simulated in SimPowerSystem.

The first model is one where 3 connected voltage sources are feeding the grid. This model is fairly similar to the designed PMSG machine using the Finite Element Maxwell model. The inductances and resistances of the generator are represented by L and R. The grid is represented by the voltage sources (4000 [V]) with the constant frequency (50 Hz), seen in Fig. 3.5. In this case it is assumed that the generators' back-EMF voltage magnitude is 4108 [V] with 80° leading which means that the internal voltage of the generator leads the infinite bus voltage.

$$P = \frac{EV}{X}\sin(\theta) \tag{3-3}$$

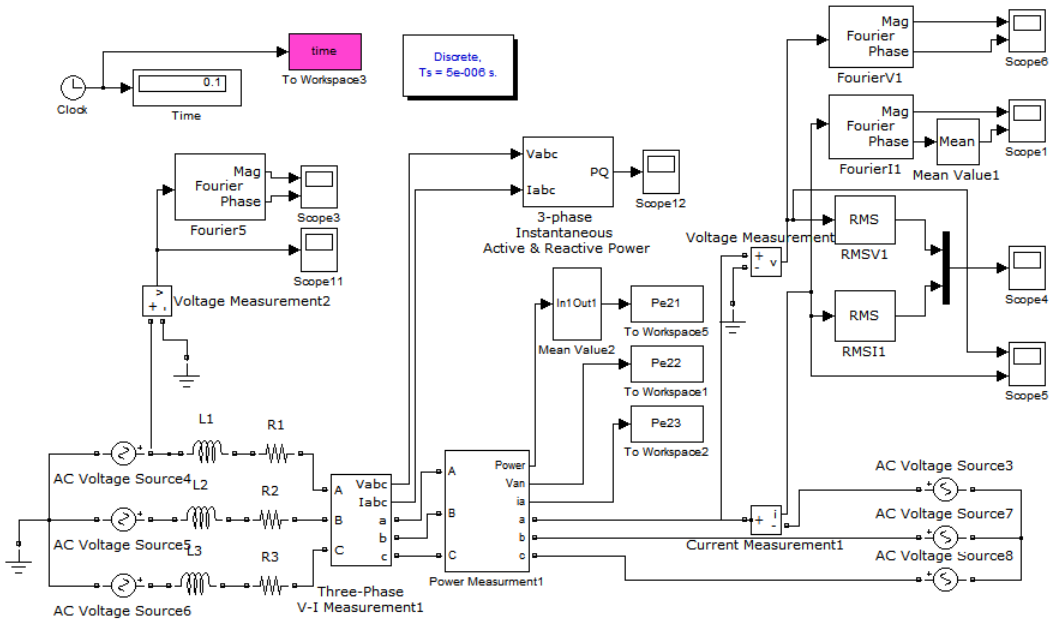

Fig. 3.5 Ideal model, 3 voltage sources connected to the DC source

The second model consists of the dynamic three phase PMSG with sinusoidal back EMF which is situated instead of 3 ideal AC voltage sources while the wind speed is higher than 12 [m/s] and the PMSG was full loaded. Fig. 3.6 shows the Simulink scheme of the PMSG connected to the grid. If the behaviour of this model agrees with the ideal model, it will be acceptable to use this model as a part of the implementation.

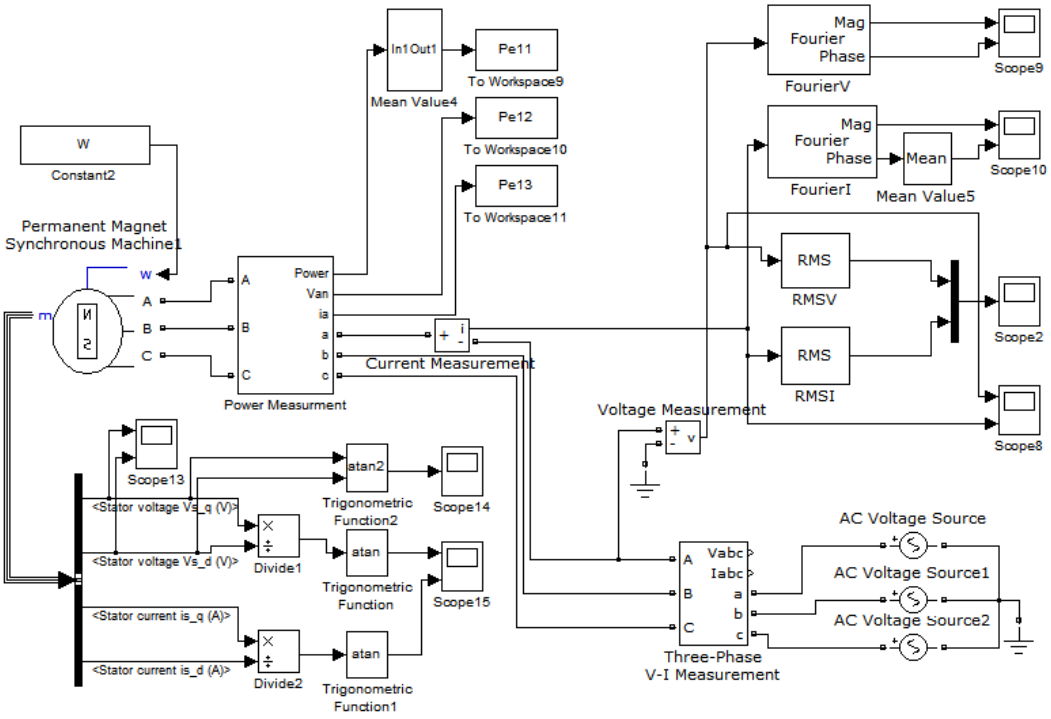

Fig. 3.6 PMSG connected to the grid

The back EMF voltage in the PMSG is aligned to the q-axis which means that the angle of the induced voltage is 90°. It should be noted that there is no control over the angle of the induced voltage, consequently to get the maximum output power according to (3-3) the difference angle between induced voltage and the grid voltage should ideally be 90°; however in this case setup it is assumed that 80°. Therefore the angle of bus voltage can be calculated as

$$\delta = \tan^{-1}\left(\frac{imag(\frac{E - I(R_s + jX)}{|V|})}{real(\frac{E - I(R_s + jX)}{|V|})}\right) = 9.8^{\circ}. \tag{3-4}$$

The applied phase angle can be observed in Fig. 3.7 which depicts the phase potential of both cases. After setting the angle of the voltage sources, the output power is shown in Fig. 3.7.b.

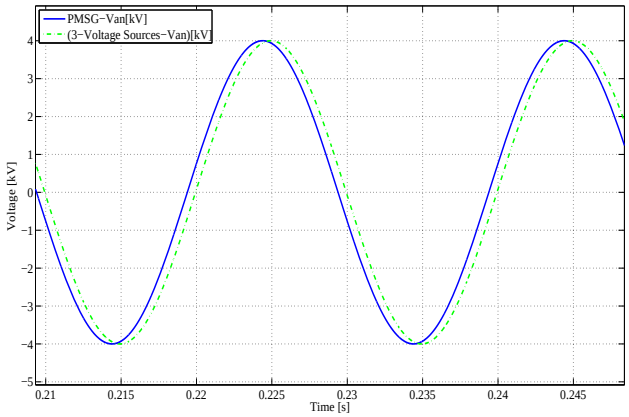

a) Phase to ground Voltage

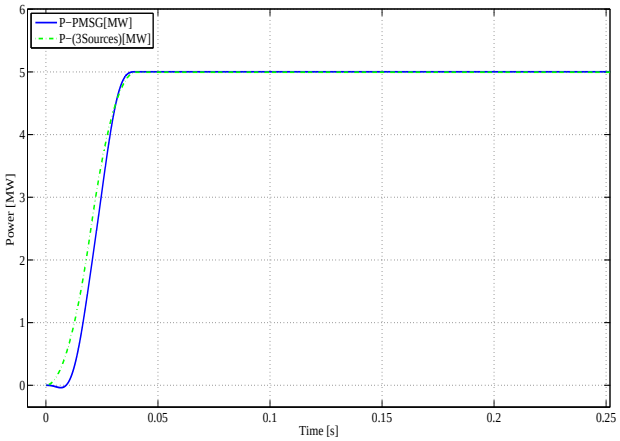

b) Output power

Fig. 3.7 Verification of PMSG output power

In order to obtain the angle of the phase current, the transformation from Cartesian coordinates to Polar coordinate has been done in the simulation part with the help of Fourier analysis. The phase currents' angles are shown in Fig. 3.8 for both cases; the observed different angle is due to the angle of the phase voltage source (9.8°) which has been calculated before to get the maximum power.

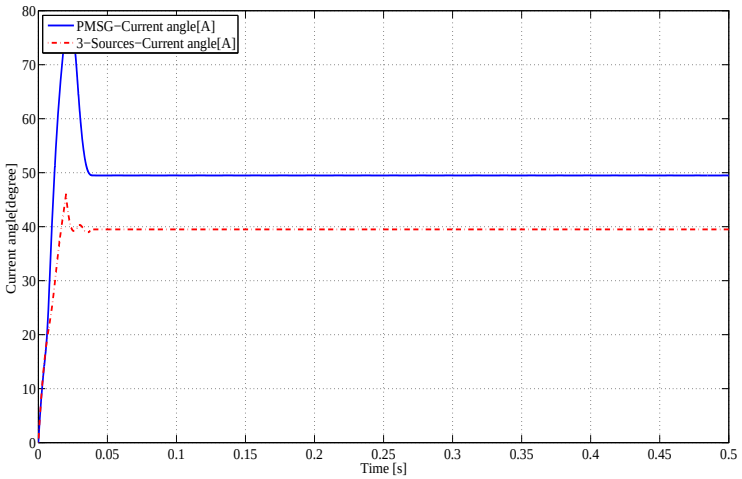

Fig. 3.8 The currents' angles in PMSG and 3-Voltage sources

However the angle of the phase voltages are different due to the constraint of controlling the angle of PMSG-back EMF, the angle between I and V is 39.5° for both cases, PMSG and 3 voltage-sources, Fig. 3.9.

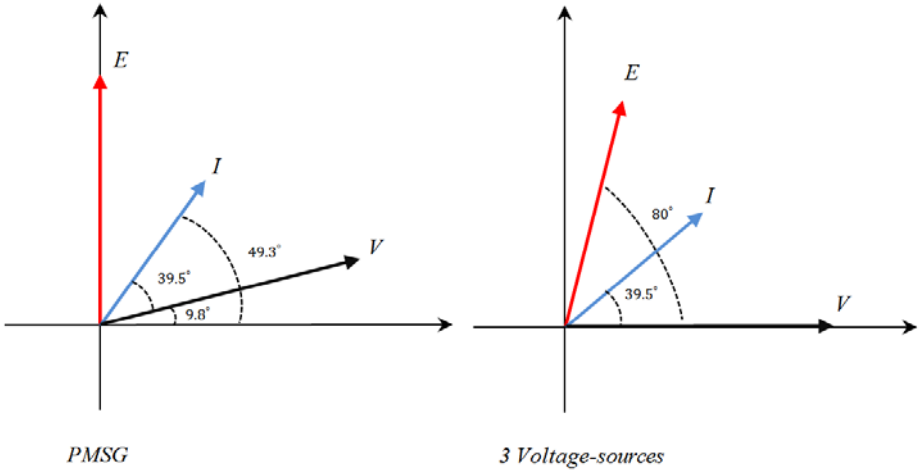

Fig. 3.9 Phasor diagram of back EMF, grid voltage and current

The results show that the implementation of PMSG works properly the same as the ideal case, thus this model can be used for the following simulations. The phase potential, the current and the power of PMSG are shown in Fig. 3.10.

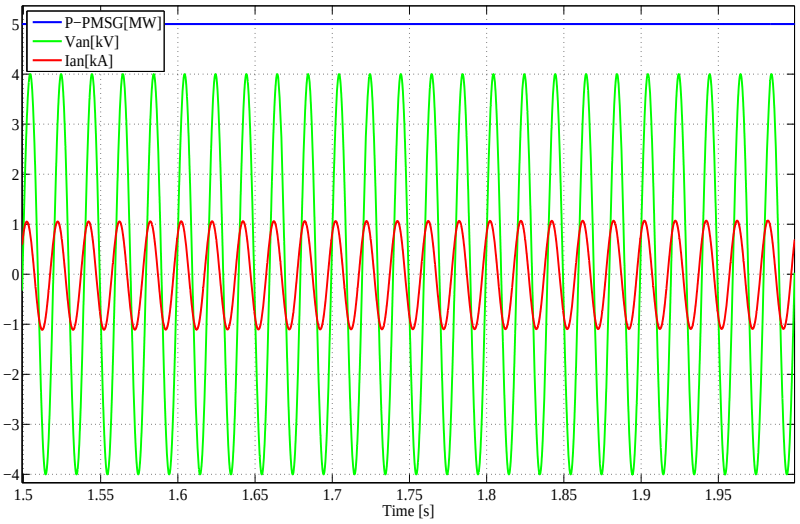

Fig. 3.10 PMSG outputs

According to the figure, the RMS phase potential is 2828.4 [V], the RMS phase current is 763.7 [A], and the power factor is 0.77.

The rotor speed, the generator speed, and output power of the PMSG for different wind speeds from 3.5 m/s to 25 m/s are shown in Table 3-2. The rotor speed reaches to the synchronous speed at 10 m/s wind speed and the maximum output power is achieved at 12 m/s wind speed. For higher wind speeds than 12 m/s the pitch control changes C_p in order to control the amount of energy converted from energy in the wind to the mechanical power on the shaft. Accordingly for the wind speed higher than 12 m/s, the electrical output power remains 5 MW.

Table 3-2 Electrical power for different wind speed

wind speed [m/s]	Rotor speed [RPM]	Generator speed [RPM]	Electrical Power [MW]
25.00	14.80	750.00	5.00
22.00	14.80	750.00	5.00
20.00	14.80	750.00	5.00
18.00	14.80	750.00	5.00

16.00	14.80	750.00	5.00
14.00	14.80	750.00	5.00
12.00	14.80	750.00	5.00
11.49	14.80	750.00	4.94
11.00	14.80	750.00	4.81
10.50	14.80	750.00	4.52
10.00	14.80	750.00	4.08
8.99	14.79	749.49	3.06
8.50	14.73	746.45	2.55
7.99	14.53	736.32	2.06
7.49	14.01	709.97	1.63
6.99	13.19	668.41	1.28
6.50	12.29	622.80	0.99
6.00	11.37	576.18	0.74
5.50	10.46	530.07	0.54
5.40	10.30	521.96	0.53
5.00	9.57	484.71	0.37
4.85	9.30	471.28	0.34
4.50	8.94	453.14	0.24
3.54	8.73	442.60	0.06

3.4 Three-phase full bridge diode rectifier

There is a possibility in SimPowerSystems to implement a Universal Bridge and then it can be set to work as a full bridge diode rectifier; but the model which is shown in Fig. 3.11 has been used in the simulation so that desired changes can be easily made

on the model and a more realistic model can be achieved. The other reason that this model is preferred is that all currents and voltages can be visualized.

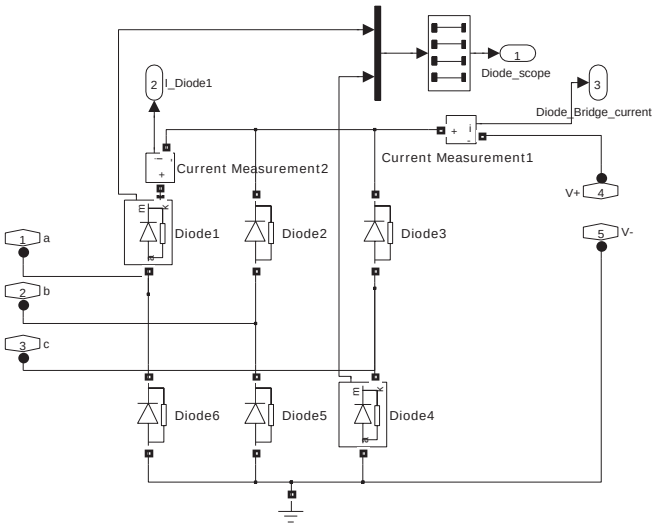

Fig. 3.11 Full bridge diode rectifier

Ports a, b, and c are connected to the PMSG and ports 4 and 5 are connected to the DC-link.

3.5 Measurement modules

To be able to study and investigate the system, line to line voltages, line potentials, currents, and phase angles should be measured. Then it becomes possible to calculate the others quantities, like active and reactive power.

Even though the various methods can be utilized to calculate the power of the generator, three methods for measurement of power have been implemented and compared in this study.

- P-Q Measurement Block
- RMS method
- Instantaneous power measurement

3.5.1 Three-Phase V-I and P-Q Measurement Blocks

The Three-Phase V-I Measurement block is provided inside the library of SimPowerSystems which should be connected in series with three-phase element then the block can output the voltages and currents. In the dialog box it is also possible to choose the measurement to be phase-to-phase voltage or phase-to-ground voltage, either in per unit (pu) values or in volts and amperes [4].

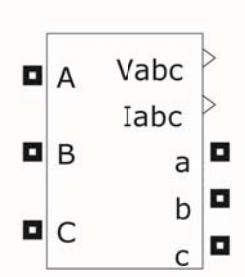

Fig. 3.12 Three-phase V-I measurement block

A complement for this block to output the active and reactive power is a 3-phase instantaneous active and reactive power block which can be found in the extra library of SimPowerSystems. This can compute the three-phase active and reactive power associated with a periodic set of three-phase voltage and currents. However its result for reactive power is not accurate when the load is not balanced and voltages and currents have harmonics [4].

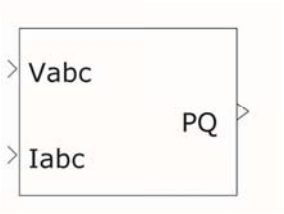

Fig. 3.13 3 phase active and reactive measurement

3.5.2 RMS method

The relationship between active power and rective power in 3-phase alternating circuits can be expressed by

$$P = 3V_{an}I_a \cos\varphi$$
$$Q = 3V_{an}I_a \sin\varphi \quad (3\text{-}5)$$
$$S = \sqrt{P^2 + Q^2}\,.$$

The RMS values of the currents and voltages can be calculated by the use of RMS block which is available in the Extras/Discerete Measerments library. The block measres the root mean spuare value of an instantaneous current or voltage which can contain the fundamental, harmonic and DC components. The angle difference of voltage and current which was obtained from the FFT block can be used for calculation of active and reactive power. It should be noted that this method can only be used if at least either the voltage or the current are sinusoidal.

3.5.3 Instantaneous power measurement

For a three-phase voltage and current the instantaneous active and reactive power can be calculated as

$$p = v_a i_a + v_b i_b + v_c i_c$$
$$q = \frac{1}{\sqrt{3}}(v_a(i_c - i_b) + v_b(i_a - i_c) + v_c(i_b - i_a)). \quad (3\text{-}6)$$

The implementation of instantaneous power measurement is shown in Fig. 3.14.

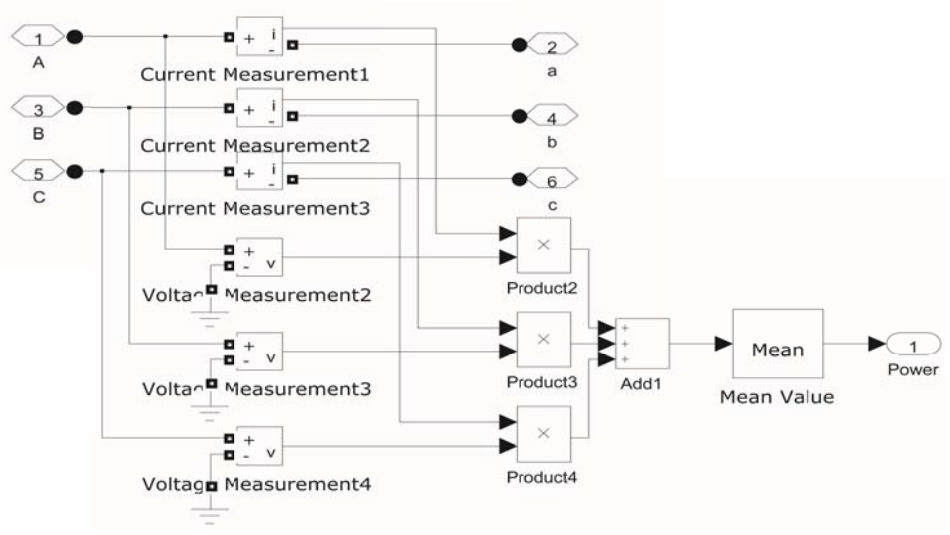

Fig. 3.14 Instantaneous power measurement

The advantage of this method is that the result is always valid and its accuracy is not dependent on the shape of neither the current nor the voltage.

In this thesis work, all mentioned methods have been used in the simulation chapter to verify the correct measurement; however the illustrated results have been taken form instantaneous power measurement method because of its high accuracy in all situations.

Chapter 4

4. Analysis Part

4.1 Simulations

To implement the generating system and analyse the system, SimPowerSystems software which operates in the Matlab Simulink has been used. SimPowerSystem is a tool which enables operators to build and simulate electrical power systems.

SimPowerSystems is an extension of MATLAB Simulink® for modeling and simulating generation, transmission and consumption which provides different components used in power systems.

The results of the SIMPLORER software is also used in this project. SIMPLORER is a software program simulating electric circuits, control and mechanical components. With SIMPLORER is possible to simulate complex power electronic and electrically controlled systems. It is helpful to analyse complicated and large-scale systems from details to the whole system [14]

This chapter explains and analyses the results of the employed SimPowerSystems models as well as the simulation.

4.1.1 Diode rectifier connected to voltage stiff

When a PMSG with a three-phase fixed magnitude voltage is connected to a DC voltage through a diode rectifier, as in Fig. 4.1, the direction of current is always from the PMSG to the grid. Besides, the magnitude of the DC link can be assumed constant for a constant wind speed; so it is reasonable to consider the output of the diode rectifier as a stiff voltage.

The transmitted power through the bridge is the production of currents and voltages. Although there is no direct control over the current in the bridge, by controlling the DC-link voltage, the current flowing from the PMSG to the DC source and consequently the

control of power transmission becomes possible. Therefore the operation point of the diode rectifier can vary from continues to discontinuous conduction mode.

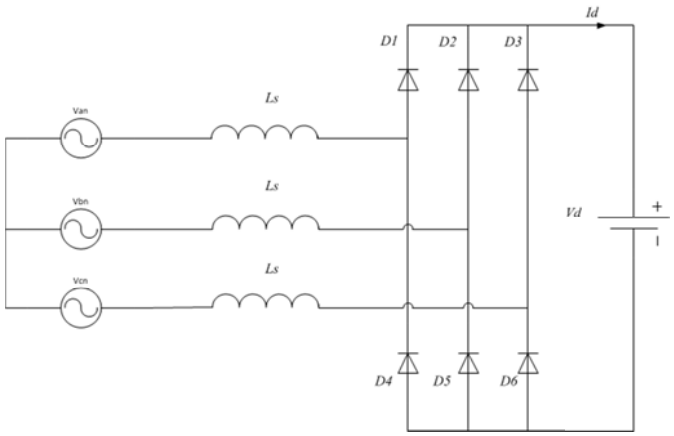

Fig. 4.1 Equivalent circuit of PMSG connected to the DC source voltage

The simulation shows that the electrical power is dependent upon the DC voltage and increasing DC voltage from zero to AC peak voltage can shift the operation point of the system from CCM to DCM as well as change the electrical transmitted power, as shown in Fig. 4.2.

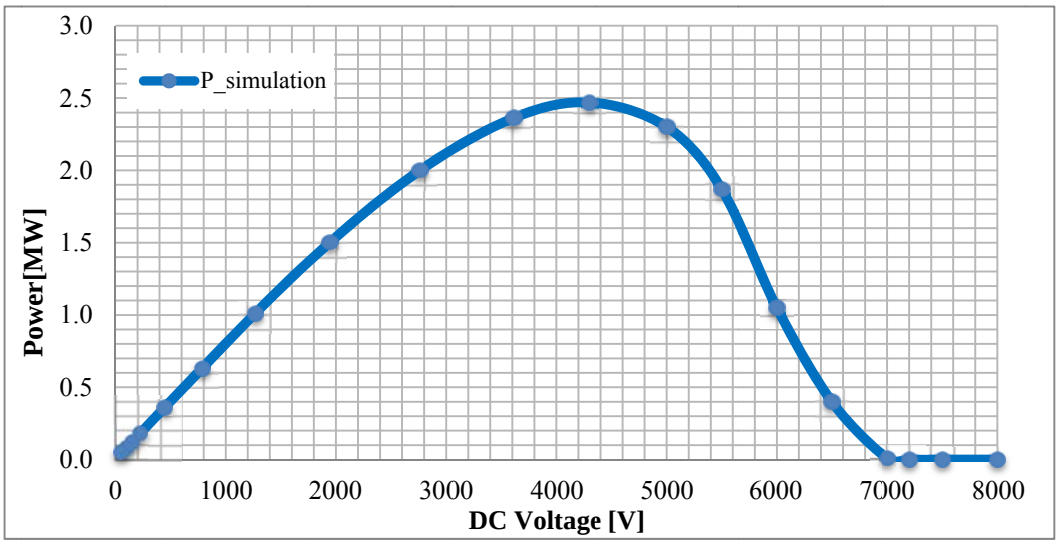

Fig. 4.2 Output power of PMSG as function of DC-link voltage, maximum rotor speed

Obviously, with diode rectifier only, a maximum of 2.5[MW] can be used. Due to this fact, no more evaluations were done using this setup. In the following the behaviour of the system in both DCM and CCM are investigated.

4.1.2 Operation of a Diode-rectifier in DCM

When the DC voltage is close to the peak AC voltage, the phase *a* current, i_a, flows discontinuously and the diode rectifier operates in DCM. Then the equivalent circuit can be simplified to Fig. 4.3. As shown in Fig. 4.4 the DC voltage is set to 6900 [V].

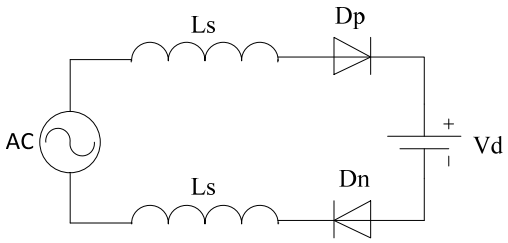

Fig. 4.3 Equivalent circuit for the diode bridge when D_p and D_n are conducting

The diode D_p starts to conduct when the potential of phase *a* equals to V_d and since the voltage over the inductor *Ls* is positive, the current flowing through the inductor increases. When the voltage over the inductor becomes zero the diode is still conducting since the diode cannot cut the inductor current and it will block the negative voltage only if the current is zero. This causes a negative voltage over the inductor. Afterwards, the inductor current decreases since there is a negative voltage over the inductor until the current becomes zero (in other words the negative voltage area equals positive voltage area).

Fig. 4.4 shows that when the phase voltage is positive, the current has two peaks according to the line to line voltages

1. $V_{ab}>V_d$
2. $V_{ac}>V_d$

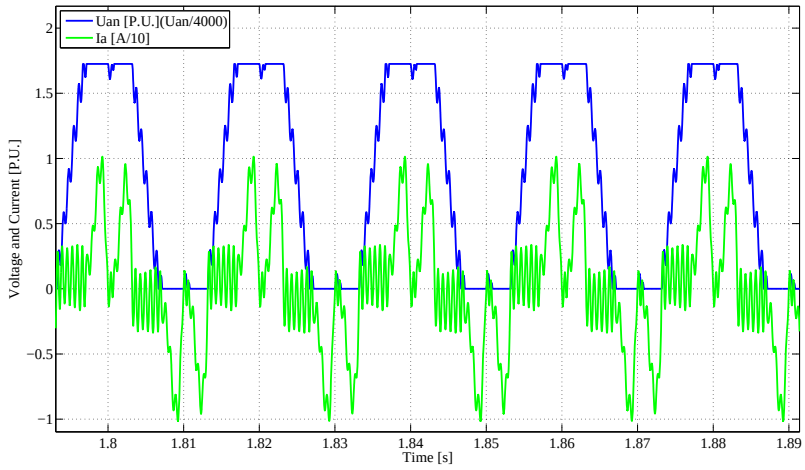

a)V_{an} and I_a

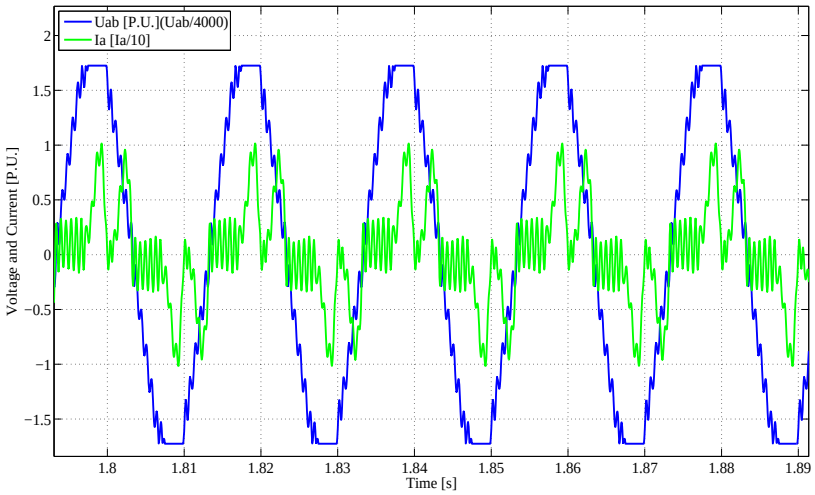

b) V_{ab} and I_a

Fig. 4.4- Voltage and current when V_d =6900 [V]

and the output DC current consists of six pulses during one period. The AC current and DC current are shown in Fig. 4.5 for V_d=6000 [V].

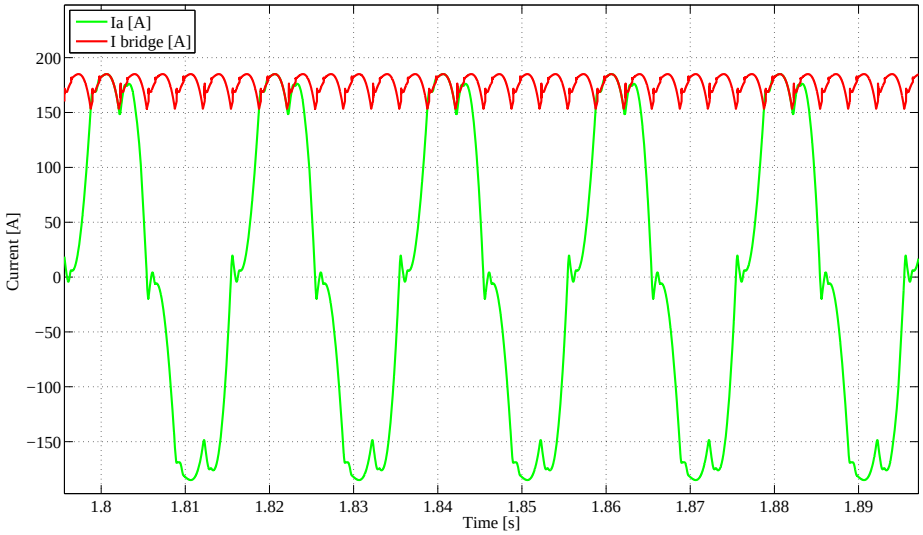

Fig. 4.5 AC current (i_a) and DC current (I_{bridge}), V_d=6000[V]

4.1.3 Operation of Diode-rectifier in CCM

A decrease on the DC voltage increases the phase-current. In other words, the AC current can be assumed sinusoidal if the voltage difference between DC source and the peak AC voltage is high enough, as in Fig. 4.6.

The diode *D1* in Fig. 4.1 starts to conduct when the peak AC voltage for phase *a* is higher than the DC voltage, so the current in phase *a* becomes positive. In the meantime, the diode *D3* is still conducting until the current in phase *c* becomes negative. *D5* is also conducting during this period Therefore phase *a* and phase *c* participate in the DC current. When the current in phase *c* becomes negative and accordingly *D3* ceases to conduct the current, phase *a* (*D1*) feeds the DC current. Afterwards, the diode *D2* conducts the current as soon as the phase *b* voltage becomes higher than the DC voltage although the diode *D1* is still conducting. Thus during a period when the DC rectified current is the summation of the currents in phase *a*, *b*, and c, then the equivalent circuit for the diode rectifier can be redrawn as in Fig. 4.7.

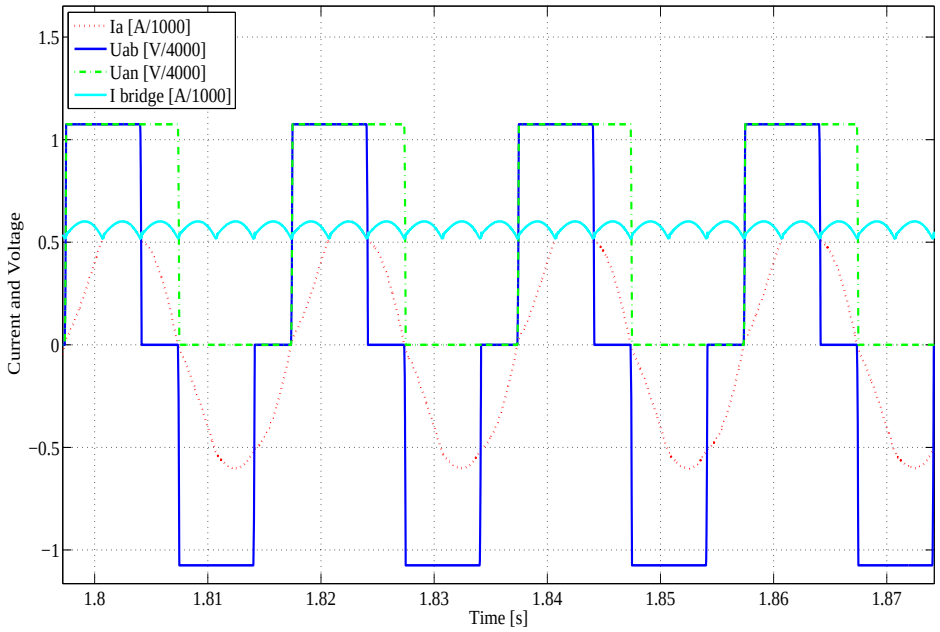

Fig. 4.6 Phase *a* current (dotted), DC current (cyan), phase *b* potential (dashed-dotted), and phase *a* to *b* potential (blue) when V_d =4300 [V]

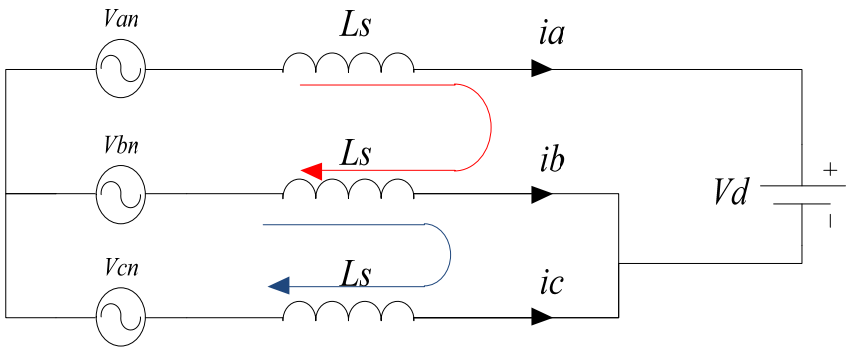

Fig. 4.7 Equivalent circuit for the diode rectifier system when the diode D1, D5, and D6 are conducting

The simulated current for this operation point is shown in Fig. 4.8.

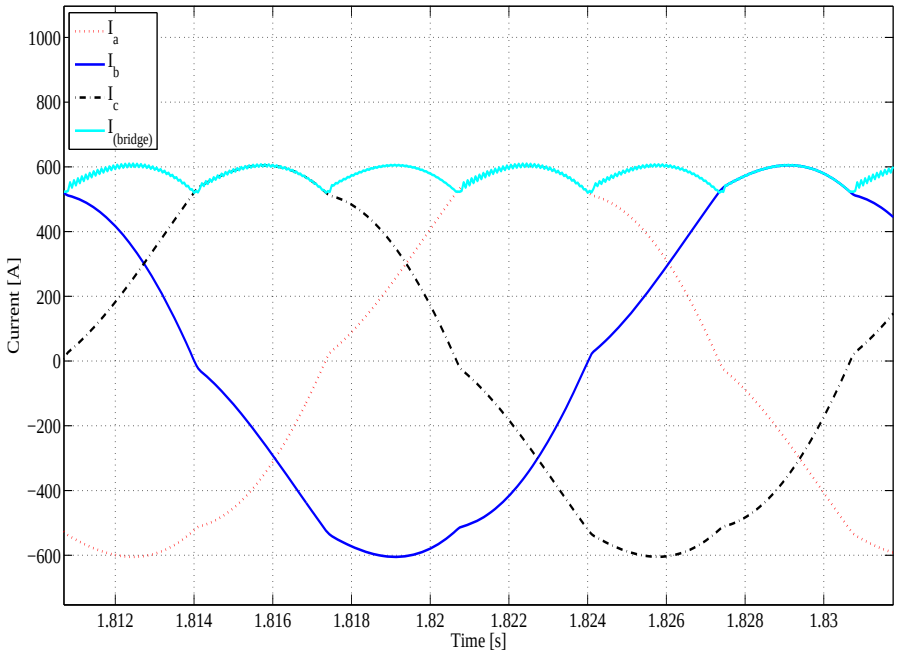

Fig. 4.8 3 phase currents and DC current

Then voltages and currents are:

$$v_{an} = V\sin(\omega t)$$
$$v_{bn} = V\sin(\omega t - {}^{2\pi}/_{3}) \quad (4\text{-}1)$$
$$v_{cn} = V\sin(\omega t - {}^{4\pi}/_{3})$$

$$i_a = I\sin(\omega t - \theta)$$
$$i_b = I\sin(\omega t - \theta - {}^{2\pi}/_{3}) \quad (4\text{-}2)$$
$$i_c = I\sin(\omega t - \theta - {}^{4\pi}/_{3})$$

During the period *D1* is conducting, one can write

$$v_{bn} - L_s\frac{di_b}{dt} + L_s\frac{di_c}{dt} - v_{cn} = 0$$
$$v_{an} - v_{bn} - L_s\frac{di_a}{dt} + L_s\frac{di_b}{dt} = V_d \quad (4\text{-}3)$$

These equations are valid when phase *a* current is at its maximum and *D1* is conducting. The phase *a* current is maximal at $\omega t = \theta + {}^{2\pi}/_{3}$. By solving the above equations at $\omega t = \theta + {}^{2\pi}/_{3}$ for θ and *I*, after some manipulations one gets [15]

$$v_{bn} - L_s\frac{di_b}{dt} + L_s\frac{di_c}{dt} - v_{cn} = 0$$

$$V\sin(\omega t - {}^{2\pi}/_{3}) - V\sin(\omega t - {}^{4\pi}/_{3}) - L_s I\omega\cos(\omega t - \theta - {}^{2\pi}/_{3}) + L_s I\omega\cos(\omega t - \theta - {}^{4\pi}/_{3}) = 0$$

$$V\,[2\sin({}^{\pi}/_{3})\cos(\omega t - \pi)] + L_s I\omega[-2\sin(-{}^{\pi}/_{3})\sin(\omega t - \theta - \pi)] = 0$$

$$-\sqrt{3}V\cos\omega t + \sqrt{3}\,L_s I\omega\sin(\omega t - \theta - \pi) = 0$$

$$\omega t = \theta + {}^{2\pi}/_{3}$$

$$I = \frac{V\sin\theta}{\omega L_s} \quad (4\text{-}4)$$

and from (4-3)

$$\mathrm{v_{an}} - \mathrm{v_{bn}} - \mathrm{L_s}\frac{\mathrm{di_a}}{\mathrm{dt}} + \mathrm{L_s}\frac{\mathrm{di_b}}{\mathrm{dt}} = \mathrm{V_d}$$

$$\mathrm{V}\sin(\omega\mathrm{t}) - \mathrm{V}\sin(\omega\mathrm{t} - {}^{2\pi}/_{3}) - \mathrm{L_s I}\omega\cos(\omega\mathrm{t} - \theta) + \mathrm{L_s I}\omega\cos(\omega\mathrm{t} - \theta - {}^{2\pi}/_{3}) = \mathrm{V_d}$$

$$\mathrm{V}\,[2\sin({}^{\pi}/_{3})\cos(\omega\mathrm{t} - {}^{\pi}/_{3})] + \mathrm{L_s I}\omega[-2\sin(-{}^{\pi}/_{3})\sin(\omega\mathrm{t} - \theta - {}^{\pi}/_{3})] = \mathrm{V_d}$$

$$V[\sqrt{3}\cos(\theta + {}^{\pi}/_{6})] + L_s I\omega\left[{}^{\sqrt{3}}/_{2}\right] = V_d$$

$$\sqrt{3}V\cos(\theta + {}^{\pi}/_{6})] = V_d - {}^{\sqrt{3}}/_{2}\, L_s I\omega$$

inserting I from (4-4)

$$\theta = \cos^{-1}\left(\frac{2V_d}{3V}\right) \tag{4-5}$$

The assumption of sinusoidal AC current is acceptable when the V is greater than V_d. Equation (4-4) shows that when the DC voltage is 4300 [V] θ is 45.74°. However, in the simulation this angle is 48°, due to the angle difference made by the diode rectifier between the phase current and the phase potential. Regarding this issue, the maximum power can be transmitted when θ equals to 48° and the DC voltage is set to 4300 [V], the power, and θ are shown in Fig. 4.9.

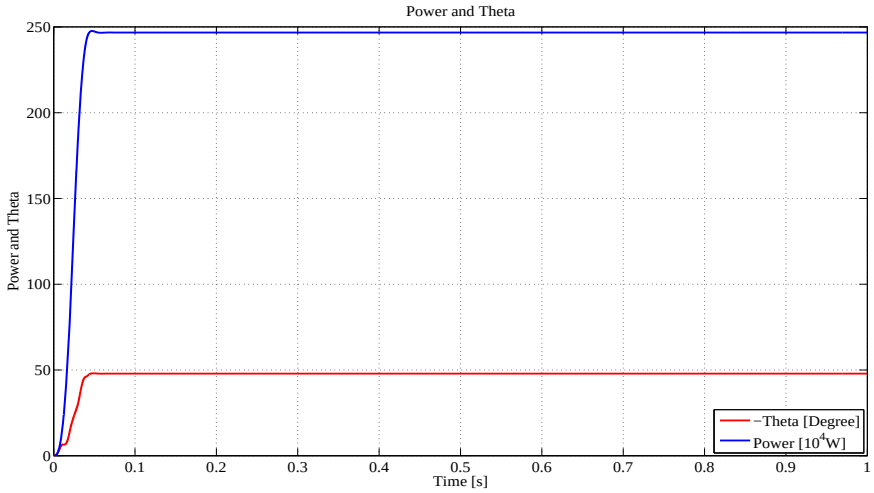

Fig. 4.9 Power and theta angle (angle between back EMF and current), V_d=4300 *[V]*

By decreasing the DC voltage the peak of AC current increases as well as the θ angle, as in Fig. 4.10, and the AC current becomes more sinusoidal. But the phase v_{an} (phase potential) and line v_{ab} (line to line voltage) decrease which are shown in Fig. 4.11.

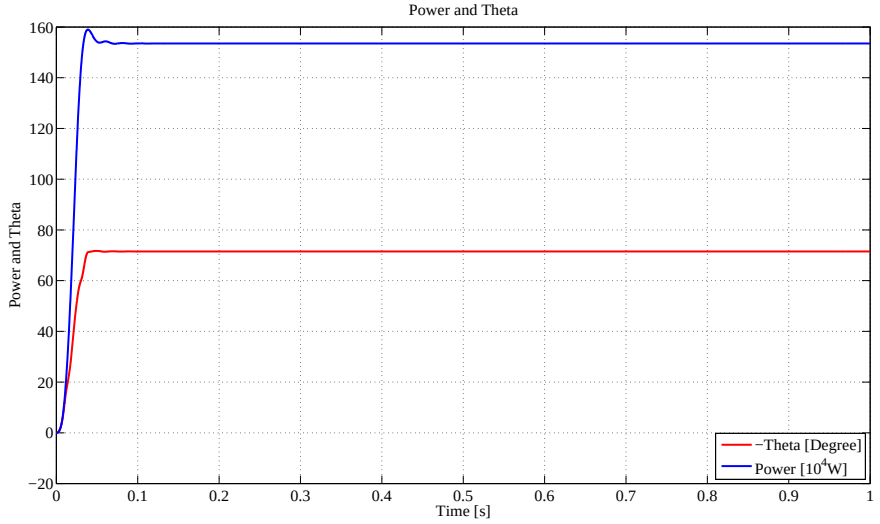

Fig. 4.10 Power and theta angle (angle between back EMF and current), V_d=2000 [V]

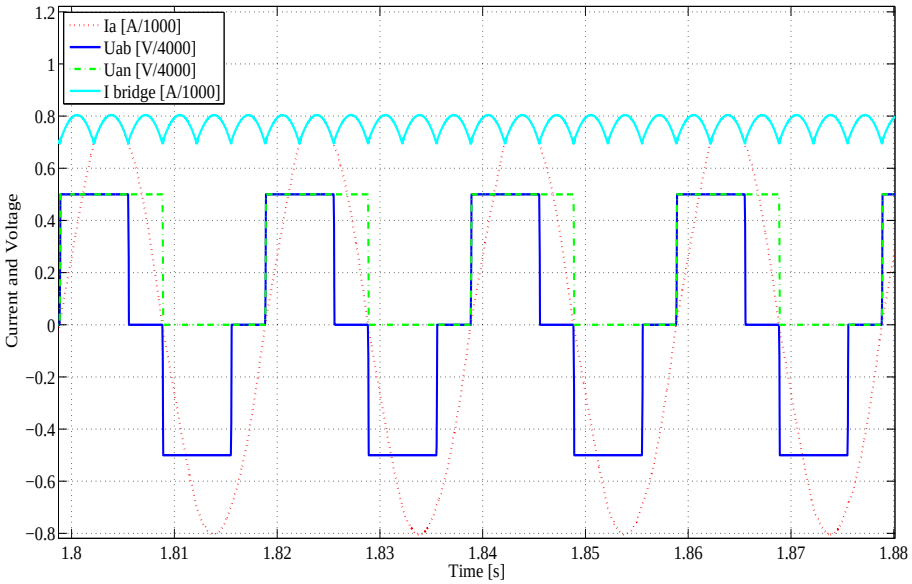

Fig. 4.11 Currents and voltages when V_d=*2000* [V]

It was explained before that the transmitted power is function of θ as can be seen in (3-3), since the angle difference between AC current and phase potential is small (2 to 3 degrees) it can be assumed that θ (the angle between voltages) is equal to δ (the angle between current and the reference voltage) Then the maximum power will be 2.5 MW. In Fig. 4.12, it can be seen that the power increases by increase of θ angle and it reaches to its maximum at 48°, then by further growth of θ the power decreases.

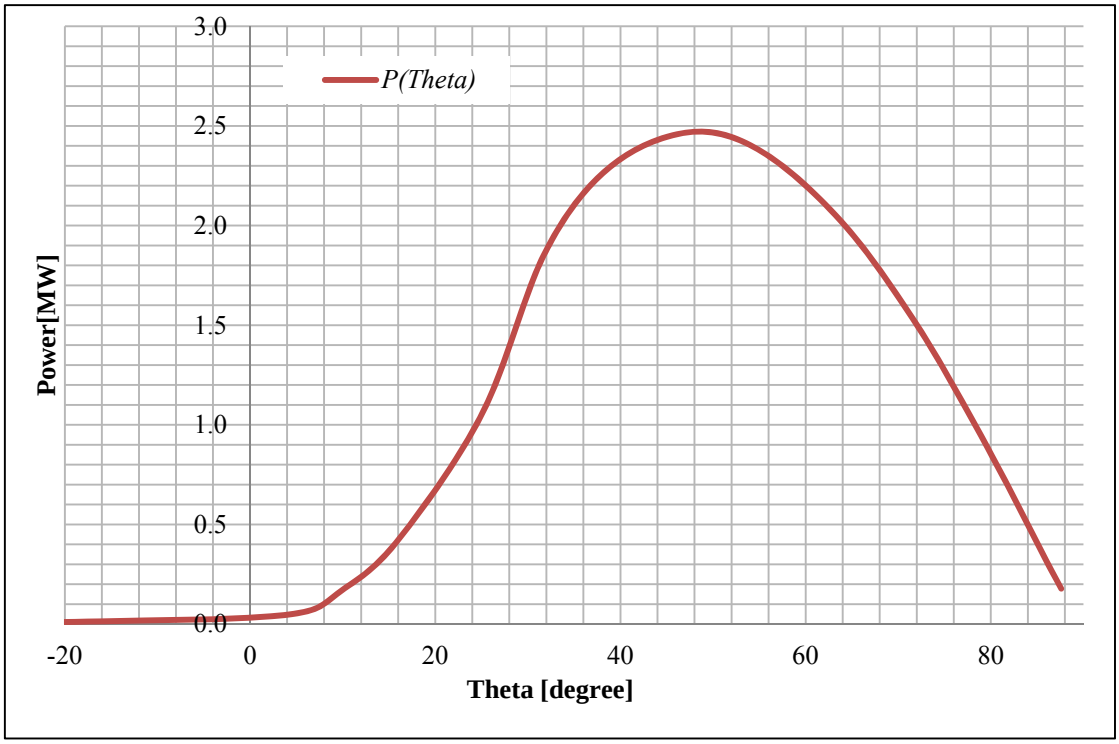

Fig. 4.12 Output power as a function of theta, according to the simulation

Connecting the PMSG to a DC source through a diode rectifier causes harmonics and potential at the neutral point. As it is depicted in Fig. 4.13 the phase to ground potential of AC source is not sinusoidal.

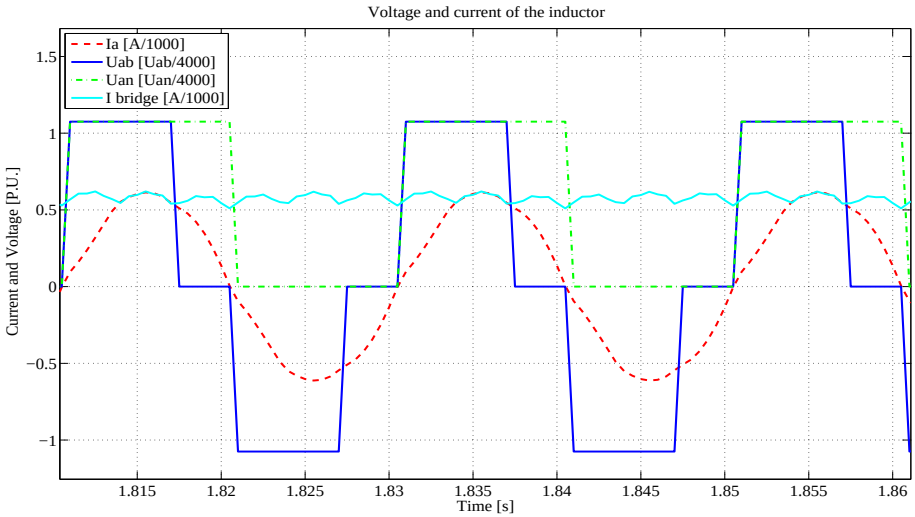

Fig. 4.13 The effect of diode rectifier on the voltages and the currents

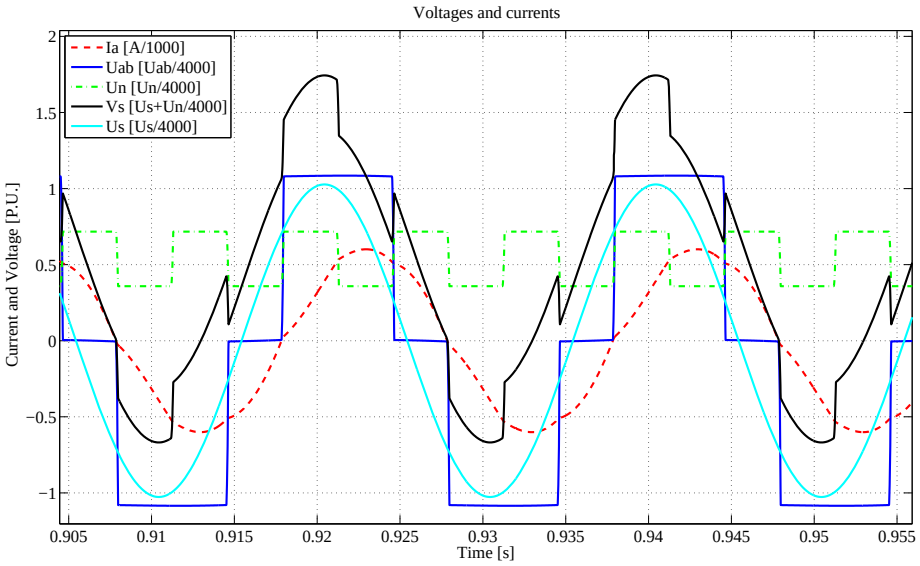

Fig. 4.14 The effect of Un on the growth of the current

The neutral potential is shown in Fig. 4.14 which boosts up the peak AC source voltage

when *D1* is conducting. When U_n is at its maximum and *D1* conducts the current rises rapidly then U_n goes to its minimum which reduces the rate of current growth, dashed red curve in Fig. 4.14.

Now it is also possible to find an expression between the DC voltage and electrical power. The 3-phase electrical power on the generator side can be written

$$P_{emf} = \sqrt{3} V_{emf} I \cos\varphi \tag{4-6}$$

where V_{emf} is line-line RMS voltage and I is phase RMS current. It can be assumed that the current goes to the diode rectifier is in phase with voltage.

$$P_{diode} = \sqrt{3} V_{diode} I_{diode} \tag{4-7}$$

The sending and receiving power should be equal so $P_{emf} = P_{diode}$ and then

$$V_{diode} = V_{emf} \cos\varphi \tag{4-8}$$

with help of (3-3)

$$P = \frac{|V_{emf}||V_{emf}\cos\varphi|}{X} \sin\theta \tag{4-9}$$

It is assumed that the voltage and current of diode are in phase, thus $\varphi = \theta$ and

$$P = \frac{|V_{emf}||V_{emf}\cos\theta|}{X} \sin\theta \tag{4-10}$$

The θ angle has been already calculated in (4-5), this leads to:

$$P = \frac{|V_{emf}|\left|V_{emf}\frac{\sqrt{2}\mathrm{V_d}}{\sqrt{3}V_{emf}}\right|}{X} \sin\left[\cos^{-1}\left(\frac{\sqrt{2}\mathrm{V_d}}{\sqrt{3}V_{emf}}\right)\right] \tag{4-11}$$

$$P = \frac{\left|\sqrt{\frac{2}{3}} V_{emf}\mathrm{V_d}\right|}{X} \sin\left[\cos^{-1}\left(\frac{\sqrt{2}\mathrm{V_d}}{\sqrt{3}V_{emf}}\right)\right] \tag{4-12}$$

$$P = \frac{\left|\sqrt{\frac{2}{3}} V_{emf} V_d\right| \left(\sqrt{1 - \frac{2{V_d}^2}{3{V_{emf}}^2}}\right)}{X} \tag{4-13}$$

The relation between electrical power and the DC voltage according to (4-13) is depicted in Fig. 4.15. However the maximum power for P-ideal is a bit higher than the maximum power from the simulation, as in Fig. 4.2, the result of equation (4-13) is according to the result from the simulation. In order to enhance the accuracy and obtain more realistic case, the angle between V_{diode} and I_{diode} should be considered. This angle varies with V_d and for this case setup it is 3° (for the maximum power and optimal V_d); then by further increase of V_d, this angle is also increased. By inserting the Ohmic losses, the curve *P2* is achieved which is in accordance with the result in Fig. 4.2. Since the ratio of resistance in comparison with the reactance of the machine is negligible both *P1* and *P2* are quite similar.

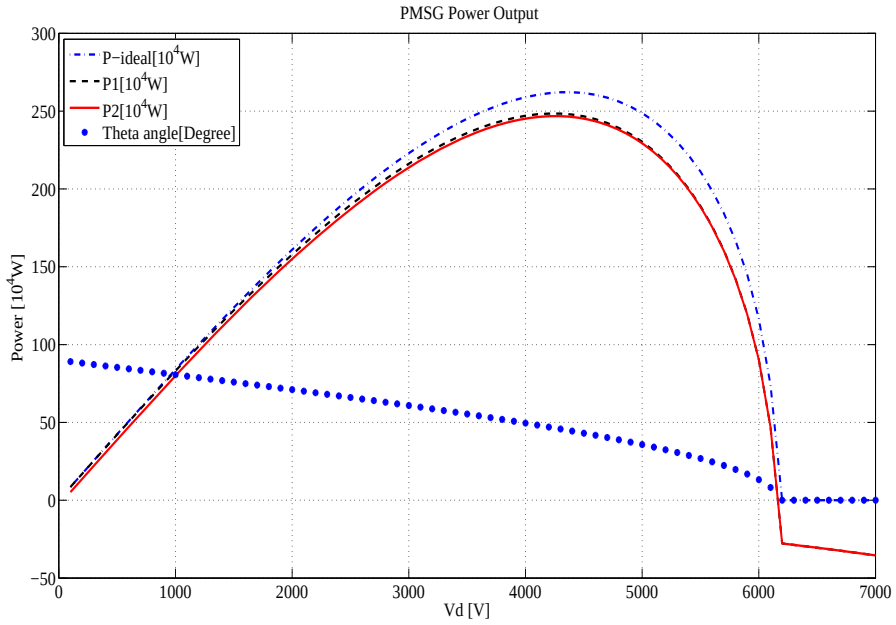

Fig. 4.15 *Ideal output power (dashed-dotted), power with* 3° *phase angle between* V_{diode} *and* I_{diode} *(dashed), more realistic power with* 3° *phase angle between* V_{diode} *and* I_{diode} *and Ohmic losses(solid)*

The analytical approach and the results from the simulation are presented in Fig. 4.16.

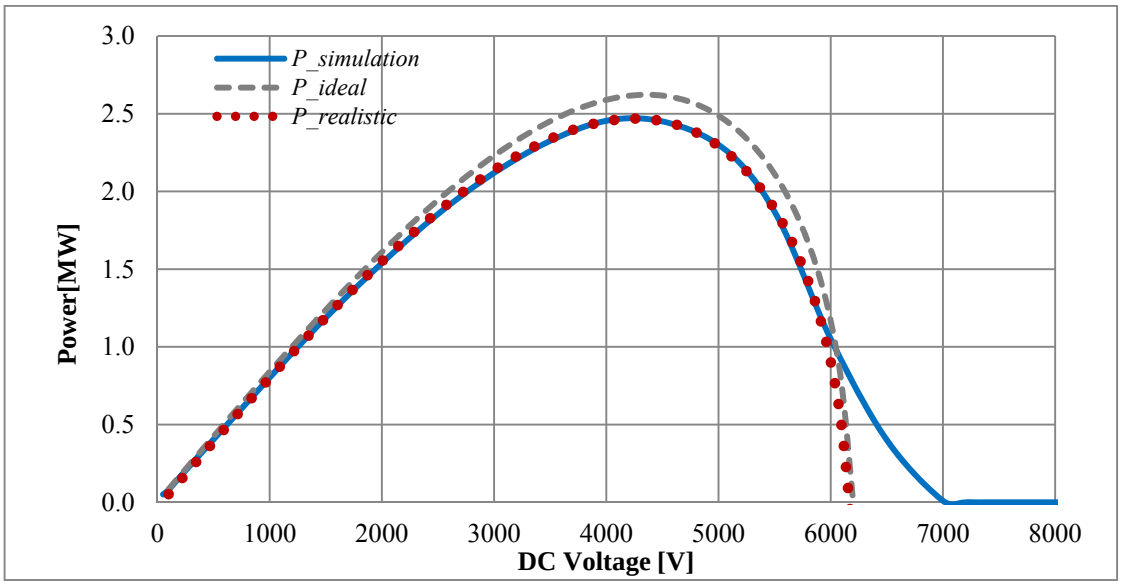

Fig. 4.16 The results of analytical approach in comparison with the results from simulation

The angle between voltage and current is due to the inductance of the generator which can be observed in simulation. Fig. 4.17 shows that in this case setup where V_d and wind speed are kept constant this angle varies by variation of the generator inductance.

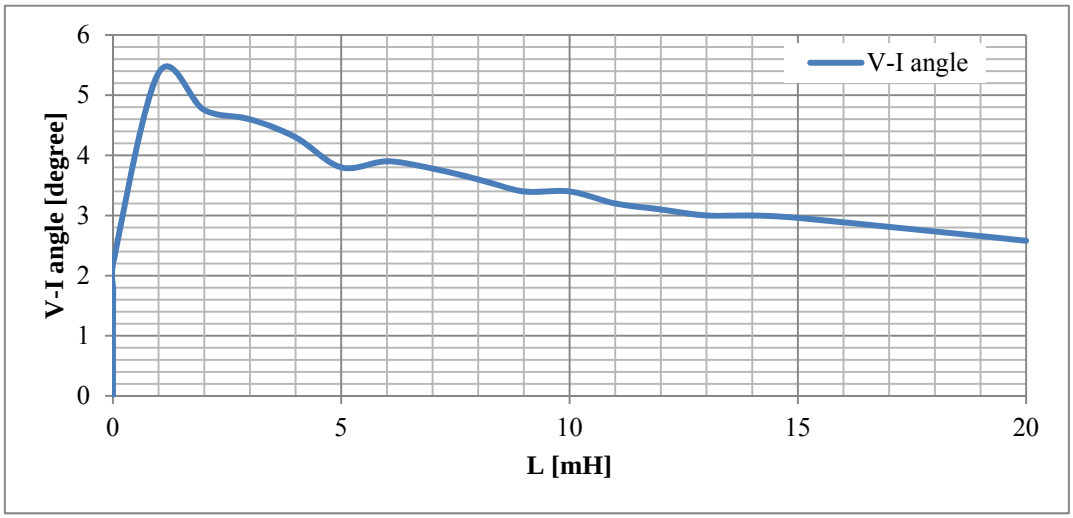

Fig. 4.17 Angle difference between voltage and current, rated operation V_d=4300 [V], wind speed=12 [m/s]

As it has been discussed before the output power is higher in *P_ideal* in comparison with the simulation, due to the fact that the angle between the source voltage and receiving voltage, θ is greater in the equation; subsequently higher power can be transmitted according to (3-3).

The trend of *P_realistic* explains that by applying the mentioned angle difference (the corrected θ) the analytical equation corresponds well to the simulations. This correction is effective when the DC voltage is less than 6000 [V], otherwise *P_realistic* will not follow the simulation. Although *P_realistic* is not required to follow *P_simulation* at every point, it is possible to re-correct the θ angle for the higher DC voltage.

4.2 Power transmission

In this part, the main idea is to look upon the DC-Link system and the output power which can be transmitted to the network. It should be noted that the maximum transmitted power of the PMSG connected to the diode rectifier is about 2.5 [MW]. Since the inductance of this generator is 15.37 [mH] and consequently the peak current is 621 [A] according to (4-4) with considering the stator resistance at rated wind speed and 4300 [V] DC voltage, extraction of 5 [MW] power from this generator is not possible.

Table 4-1 The result of simulation for the PMSG with diode rectifier for different wind speed

Wind speed [m/s]	4	6	8	10	12	14	16	18	20	22	24
Rotor speed [RPM]	444	576	746	750	750	750	750	750	750	750	750
V_d [V]	100	445	1265	2760	4300	4300	4300	4300	4300	4300	4300
P [MW]	0.08	0.36	1.01	2.00	2.47	2.47	2.47	2.47	2.47	2.47	2.47
I_{DC} [A]	824	812	795	724	580	580	580	580	580	580	580
V-I angle [degree]	0	0	0	1	3	3	3	3	3	3	3
Peak Line to Line voltage [V]	100	445	1265	2760	4300	4300	4300	4300	4300	4300	4300

I_{AC} (peak) [A]	850	847	832	759	621	621	621	621	621	621	621

Table 4-1 presents the result of the diode rectifier simulation for the different wind speed. As can be seen, the maximum DC current is 825 [A] at minume wind speed and the maximum power can be extracted from the wind energy at 12 [m/s] win speed.

4.2.1 Series compensation

As already described, the power transfer capability depends on the inductance of the generator. By using a series capacitor, the imaginary part of the impedance of the generator seen from the DC side can be reduced and the loading of the system can be increased. Therefore this can increase the transmittable power in the system. Fig. 4.18 shows the increase in transmittable power by decreasing the inductance of the system.

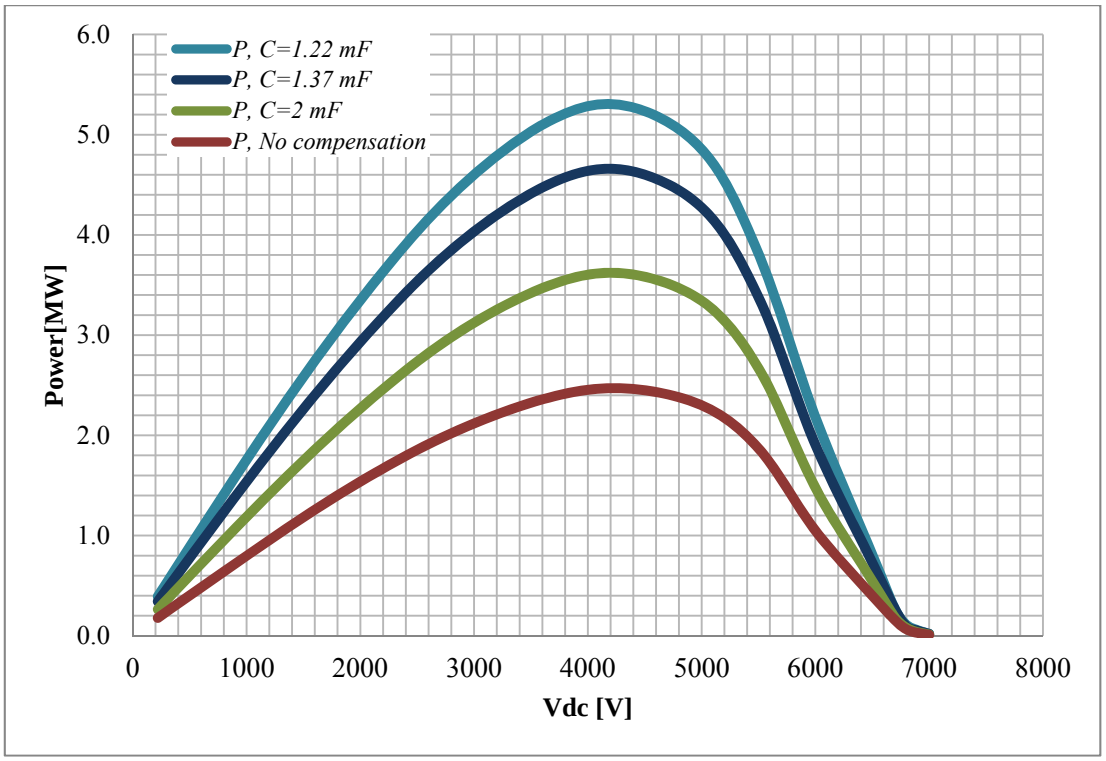

Fig. 4.18 The effect of series compensation on power

As already described, the transferred power depends on the inductance of the generator; by using series capacitors the imaginary part of the impedance of the generator can be reduced and this enhances the transmittable power. The effect of series capacitors on increase of power transfer can be expressed as

$$P = \frac{\left|\sqrt{\frac{2}{3}} V_{emf} V_d\right| \left(\sqrt{1 - \frac{2{V_d}^2}{3{V_{emf}}^2}}\right)}{X - X_c} \quad (4\text{-}14)$$

where X_c is the inserted capacitanc.

Since the 1.45 [mF] capacitor provides the required rated power of the PMSG, as seen in**Error! Reference source not found.**, it has been used for the simulation assuming all 3 phases to be equipped. The result of operating conditions for the whole system are reported in Table 4-2.

Table 4-2 The effect of series compensation (C=1.22[mF]) on the PMSG with diode rectifier

Wind speed [m/s]	4	6	8	10	12	14	16	18	20	22	24
Rotor speed [RPM]	444	576	746	750	750	750	750	750	750	750	750
V_d [V]	45	205	570	1150	3700	3700	3700	3700	3700	3700	3700
P [MW]	0.08	0.36	1.01	2	5.1	5.1	5.1	5.1	5.1	5.1	5.1
I_{DC} [A]	1800	1790	1779	1749	1394	1394	1394	1394	1394	1394	1394
V-I angle [degree]	0	0	0.7	1.6	3.8	3.8	3.8	3.8	3.8	3.8	3.8
Peak Line to Line voltage [V]	45	205	570	1150	3700	3700	3700	3700	3700	3700	3700
I_{AC} (peak) [A]	1870	1865	1858	1829	1463	1463	1463	1463	1463	1463	1463

There is an important relataion between the capacitor reactive power and its size and cost. The reactive power of the capacitor is

$$Q = I_{RMS}^2 X_c = \frac{V_{RMS}^2}{X_c} \tag{4-15}$$

In this case setup, the RMS current of the capacitor is 1035 [A], for 3700 [V] DC link voltage and rated speed, then the reactive power provied by the capacitor is 2.8 [MVar].

4.2.2 Shunt compensation

The shunt compensation is a way to deal with voltage dip and stability enhancement on a long transmission line. But in this project it can compensate the voltage drop on the inductance of the PMSG, alternatively it boosts V_{diode} in (4-8) to about V_{emf}; moreover it can supply the capacitive current. The shunt reactive compensation can increase the steady-state transmittable power and it also acts as a filter for harmonics. However it is not as effective as series compensation for increasing the capability of the power transmission.

If the DC voltage is kept constant, by injecting the reactive current through the shunt capacitor the output power can be influenced; as shown in Fig. 4.19, it is possible to get 3.425 [MW] power by implementering 106 [uF] delta-connected capacitors.

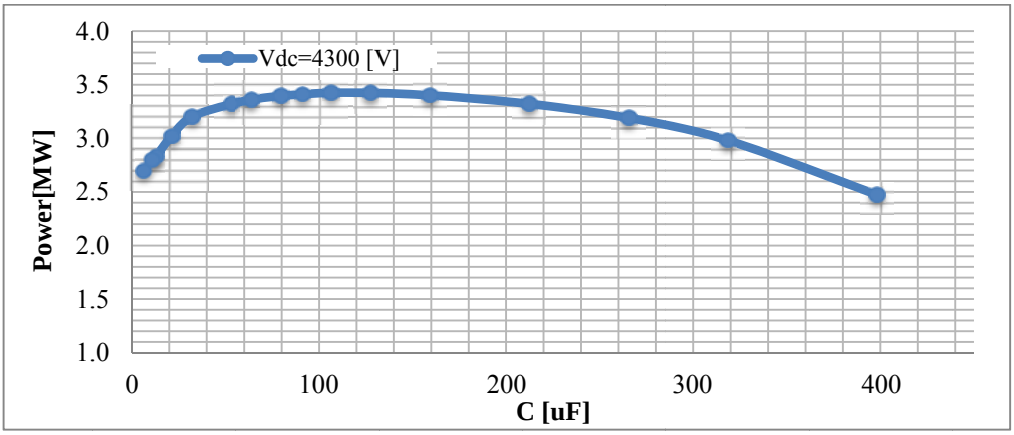

Fig. 4.19 Shunt capacitor and electrical output power, maximum rotor speed

Fig. 4.20 shows the electrical power as a function of DC voltage for both with and without shunt compensation. It can be seen that in order to get 5 [MW] power the DC voltage should

be 7000 [V] while a shunt capacitor bank with C=106 [uF] is connected to system and the DC voltage should be 8000[V] if C=80 [uF] is connected.

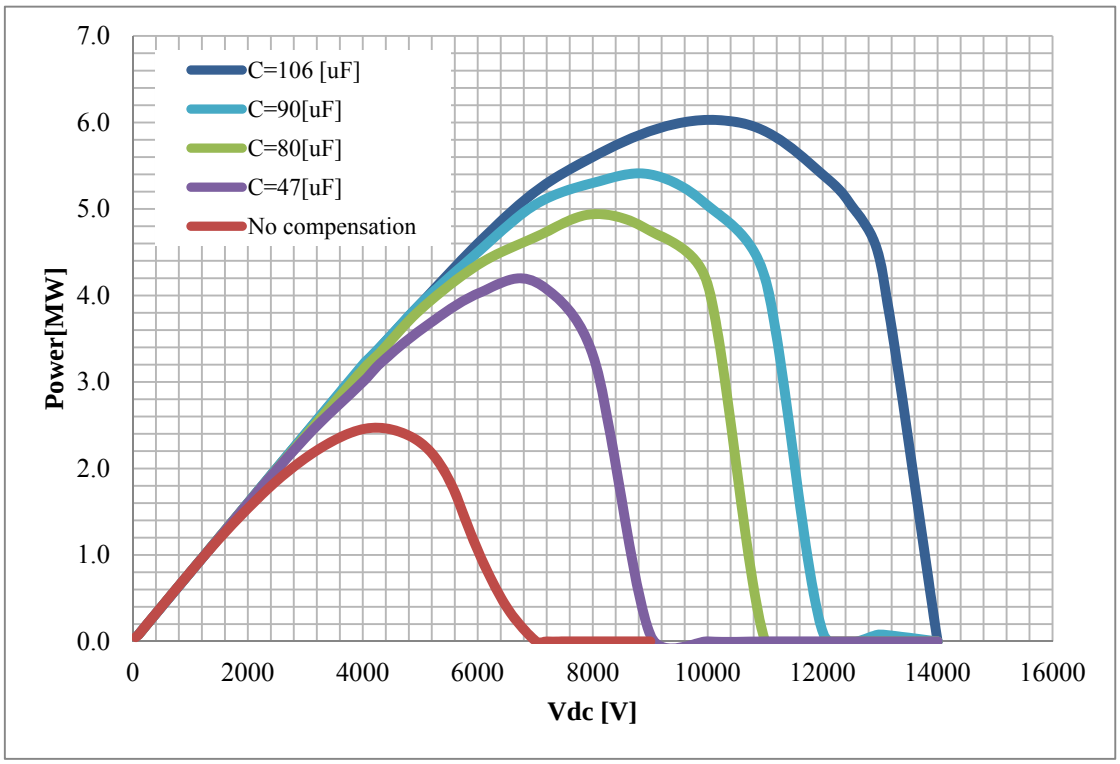

Fig. 4.20 Output power with and without shunt compensation

The simulation results with a 100 [uF] shunt capacitor for each-phase are reported in Table 4-3 which shows that 5 [MW] power can be achieve at higher DC voltage (7000 [V]) while the DC voltage for series compensation is 4300 [V] to get the same output power. The reactive power provided by 100 [uF] shunt capacitor is 1.06 [MVar] when the RMS line to line voltage is 5790 [V].

Table 4-3 The effect of shunt compensation (C=100[uF]) on the PMSG with diode rectifier

Wind speed [m/s]	4	6	8	10	12	14	16	18	20	22	24
Rotor speed [RPM]	444	576	746	750	750	750	750	750	750	750	750

V_d [V]	100	445	1265	2760	7000	7000	7000	7000	7000	7000	7000
P [MW]	0.08	0.36	1	2.2	5.14	5.14	5.14	5.14	5.14	5.14	5.14
I_{DC} [A]	824	813	805	801	733	733	733	733	733	733	733
V-I angle [degree]	3.4	8.3	15.97	23.4	37	37	37	37	37	37	37
Peak Line to Line voltage [V]	100	445	1265	2760	7000	7000	7000	7000	7000	7000	7000
I_{AC} (peak) [A]	852	858	883	934	992	992	992	992	992	992	992

4.2.3 Effect of core saturation

The inductance of the machine is determined by its dimentions and the material of which it is formed. The B-H curve of the PMSG, seen in Fig. 4.21, shows that the inductance of the machine varies with load; at full load operation the core of the PMSG becomes saturated thereby the inductance of the PMSG decreases.

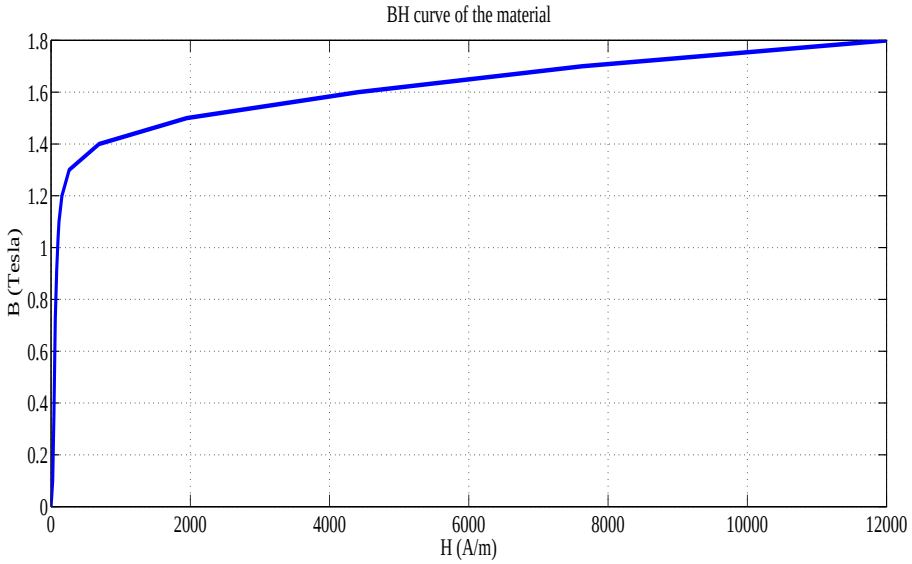

Fig. 4.21 Magnetic flux density and magnetic field

The reduction of the inductance causes the increase of phase current, consequently the output power can increase more. However this reduction of inductance is valid just for the case when the increase of current is so that the core becomes saturated.

In this work, since the core saturation happens in both, diode rectifier and IGBT converter scenarios, thereby it is possible to compare two scenarios without considering the effect of core saturation.

4.3 Loss determination

In the previous sections, the diode rectifier has been introduced with simulations using models with ideal diodes. In this section, data for commercial diode modules provided in the appendix are used.

The losses for both the diode rectifier and the IGBT rectifier are going to be studied and compared. However, additional losses as losses in cables and losses for cooling are not included in the loss calculation.

4.3.1 Diode losses

Diode losses consist of both conduction losses and switching losses. However, for the diode rectifier the conduction losses are dominant and the switching losses can be neglected in comparison with conduction losses; due to the natural commutation and after the fact that the commutations occur at low frequency. The conduction losses can be calculated using the forward voltage drop and current during the on-state period. The on-state characteristics for the diodes are available in the data sheets. Then the conduction losses can be calculated as in (2-5).

The forward voltage V_f is shown in a graph as a function of forward current I_f in the data sheet which is depicted in Fig. 4.22.

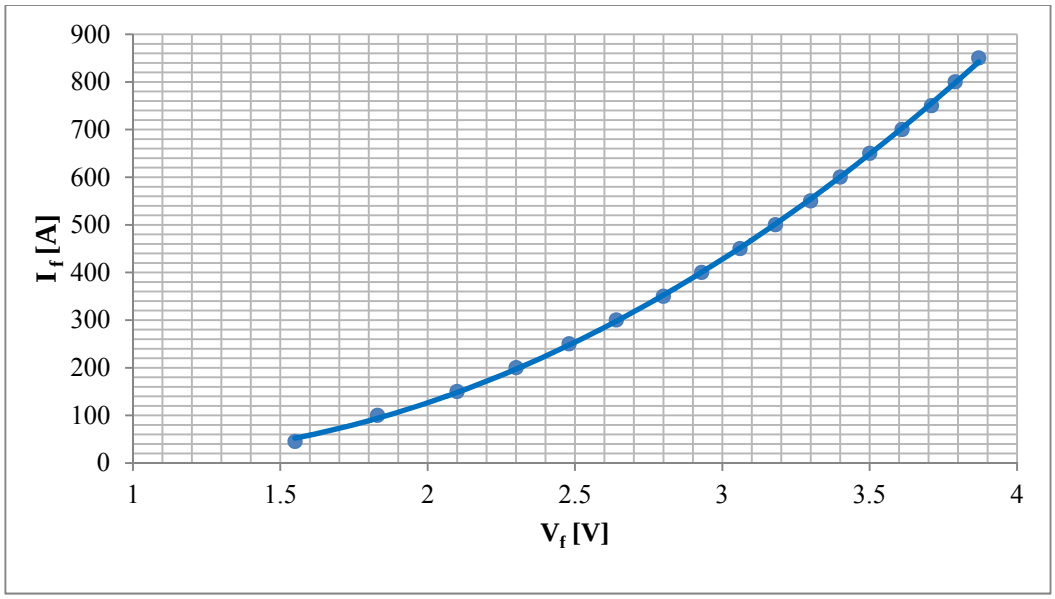

Fig. 4.22 Forward Characteristics of the diode at T=125° C

The shown forward voltage in the diode can be estimated as

$$V_f = -2 \times 10^{-6} I_f^2 + 4.6 \times 10^{-3} I_f + 1.4124 \quad 4\text{-}16)$$

The values for the constants in (4-16) can be obtained from the datasheet for the diode (as seen in Fig. 4.22). Consequently, the conduction losses in the diode are then given by

$$P_{diode} = V_f I_f = -2 \times 10^{-6} I_f^3 + 4.6 \times 10^{-3} I_f^2 + 1.4124 I_f \quad 4\text{-}17)$$

Each diode module selected has the capability to conduct 1200 A current and block 6500 voltage. To handle the rated operation point and also to consider the safety margin, 8 diodes in two parallel branches have been implemented in each leg of the diode rectifier, the diode rectifier has 3 legs. Thus, the total loss of the diode rectifier with series compensation for the rated speed and 3700 DC voltage will be $15.3 \times 10^3 [W]$.

However, in sections 4.3.4 and 4.4, it is explained that how the selection of equilibrium DC link voltage can reduce the losses and increase the efficiency of the system for both shunt and series compensations.

4.3.2 IGBT-converter losses

The used IGBT module is the 6500V/750A ABB HiPak [16]. To get the desire voltage, 10 kV, 2.78 numbers of series and 1.66 parallel IGBT-modules are used which is a fractional number [12].

As can be seen in Fig. 4.23, the switching losses are about 4 times higher than the conduction losses and the total losses of the IGBT-converter are 64.6 [kW] for wind speed higher than 12 [m/s] [12].

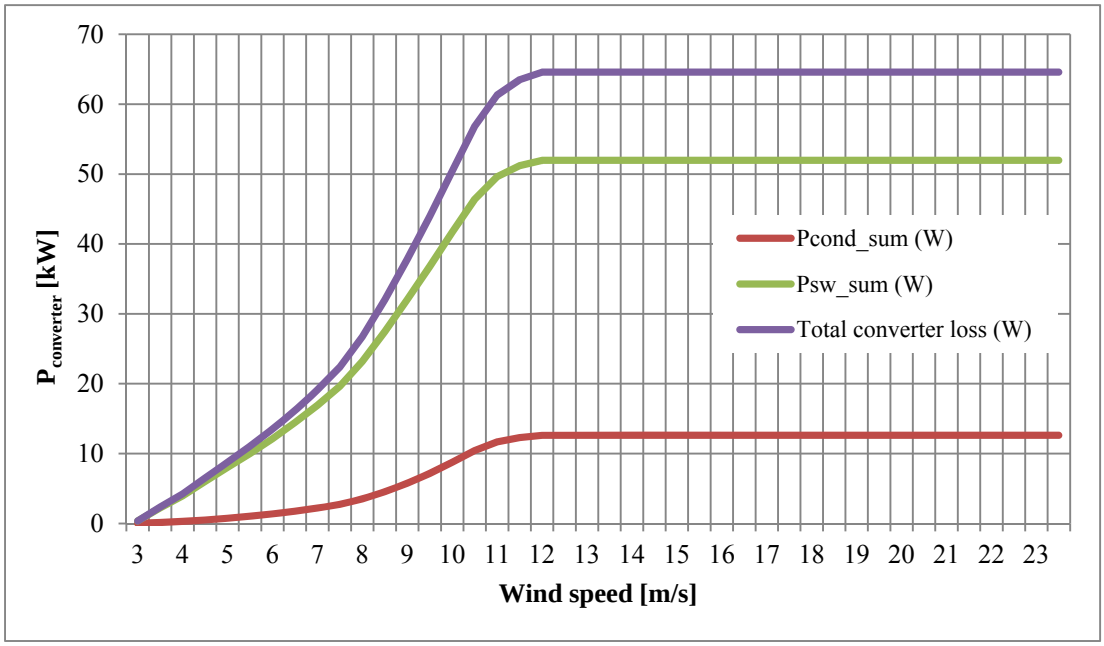

Fig. 4.23 Converter losses for a converter built up using the IGB module 6500V/750A, V_d=10 [kV]

4.3.3 Generator losses

As was mentioned in Section 2.5.3 the main losses for the used PMSG in this work consists of only copper losses and iron losses of the machine.

The Iron loss of the machine has been considered to be purely dependent on the speed, according to (2-12). Therefore, it can be seen that in Fig. 4.24, the iron losses are the same for

all three scenarios, No compensation, Series compensation, and Shunt compensation.

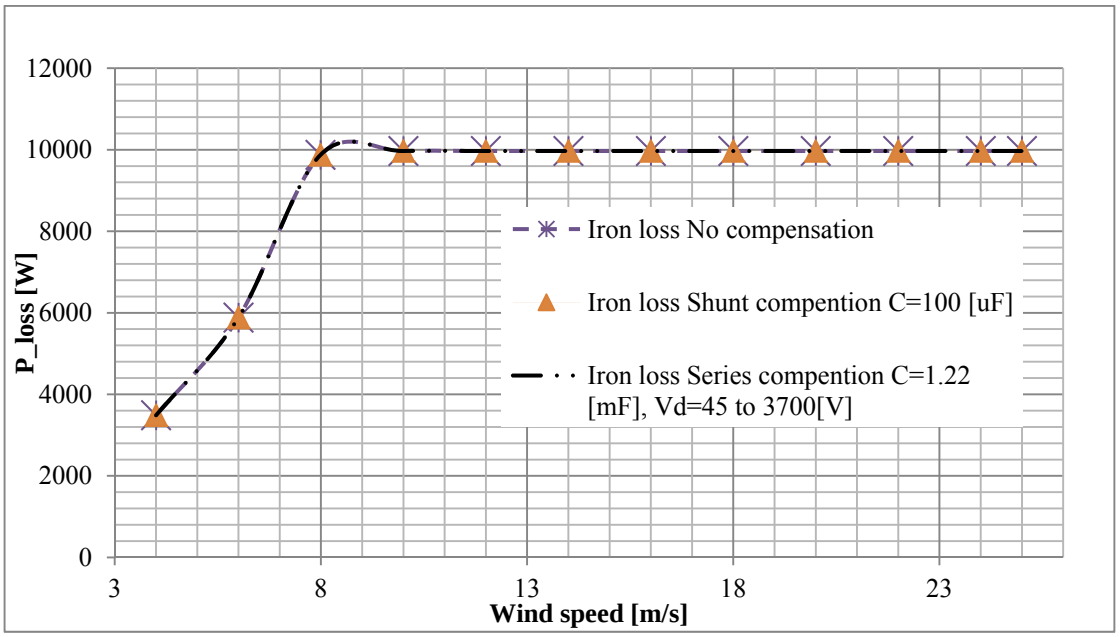

Fig. 4.24 Iron losses of the machine for different configurations

The simulation results with a 1.22 [mF] series capacitor for each-phase are reported in Table 4-4 which shows that the effect of the series compensation on currents and voltages for different wind speed and Table 4-5 presents the simulation results of the shunt compensation. Accordingly, the machine copper losses can be calculated for these cases.

Table 4-4 The effect of series compensation (C=1.22[mF]) on currents and V_{DC} with diode rectifier

Wind speed	4	6	8	10	12	14	16	18	20	22	24	25
Power	0.08	0.36	1.01	2	5.1	5.1	5.1	5.1	5.1	5.1	5.1	5.1
V_{DC}[V]	45	200	570	1130	3700	3700	3700	3700	3700	3700	3700	3700
I_{AC} (Peak)	1864	1865	1850	1828	1463	1294	1294	1294	1294	1294	1294	1294
I_{RMS} [A]	1320	1319	1308	1294	1035	1035	1035	1035	1035	1035	1035	1035

Table 4-5 The effect of shunt compensation (C=100[uF]) on currents and V_{DC} with diode rectifier

Wind speed	4	6	8	10	12	14	16	18	20	22	24	25
Power	0.08	0.36	1.01	2	5.1	5.1	5.1	5.1	5.1	5.1	5.1	5.1
V_{DC}[V]	100	445	1265	2760	7000	7000	7000	7000	7000	7000	7000	7000
I_{AC} (Peak)	852	858	883	934	992	992	992	992	992	992	992	992
I_{RMS} [A]	602	606	622	654	700	700	700	700	700	700	700	700

Fig. 4.25 shows that the copper losses in Shunt compensation scenario increases by raising the wind speed, due to the increase of current in the stator winding. Series compensation increases the current flowing in the stator windings, as can be seen in Table 4-4, due to reducing the effect of machine inductance; therefore in this setup with 3700[V] DC link voltage, Series compensation has the highest copper losses.

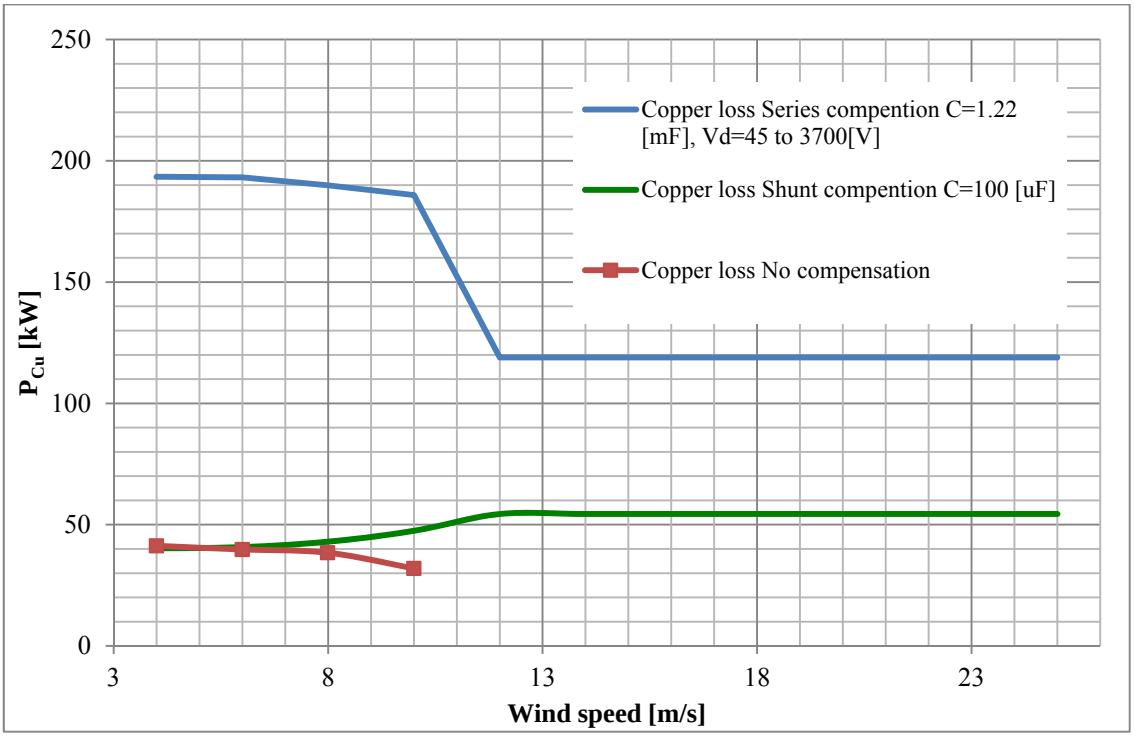

Fig. 4.25 Copper losses of the machine for different configurations

However, in Series compensation, the copper losses at higher wind speed and higher power decreases with increasing the voltage, the series compensation with this operation point (V_{DC}=3700[V]), very high copper losses, is impractical.

Since, the No compensation case cannot provide 5MW output at rated operation, this case can be compared to the other cases up to 10[m/s] wind speed while all cases provide 2 MW power. It is clear that the series compensation scenario with higher copper losses has the maximum total machine losses for the investigated PMSG, as can be seen in Fig. 4.26.

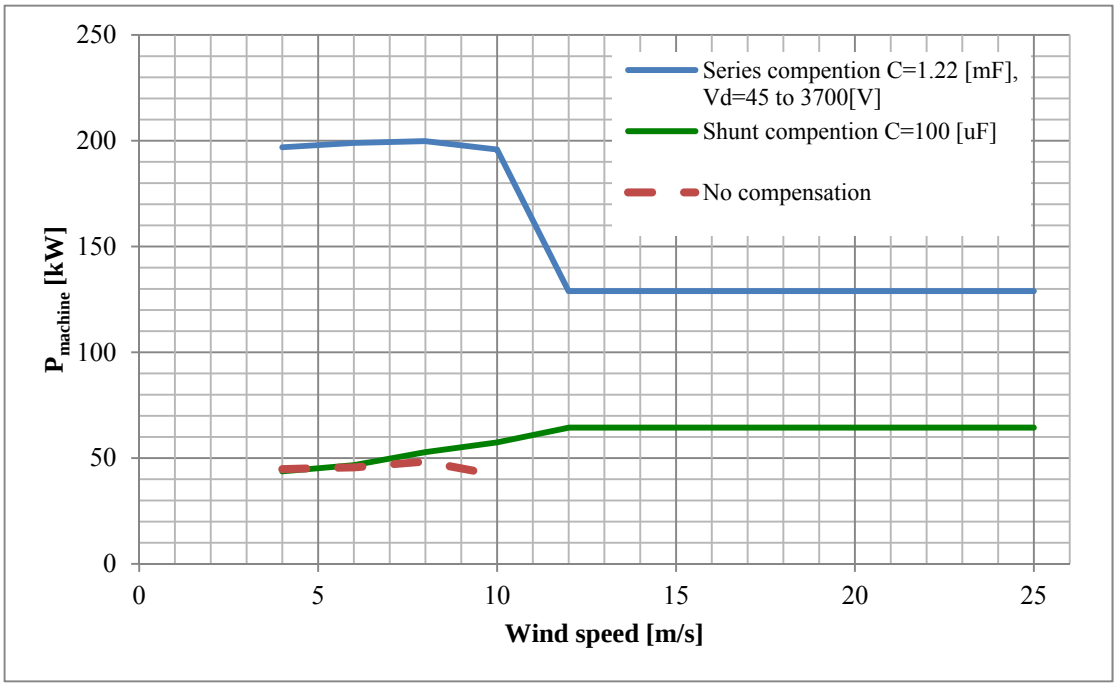

Fig. 4.26 Total machine losses for different configurations with diode rectifier

It is noticeable that the machine losses shown in the figure are too high and it is crucial to find a way to reduce the losses; otherwise the production will not be beneficial.

The generator losses, for the IGBT-converter scenario, for different wind speed and different DC link voltage are shown in Fig. 4.27 [12]. It can be seen that the copper losses are much higher than the iron losses in the machine.

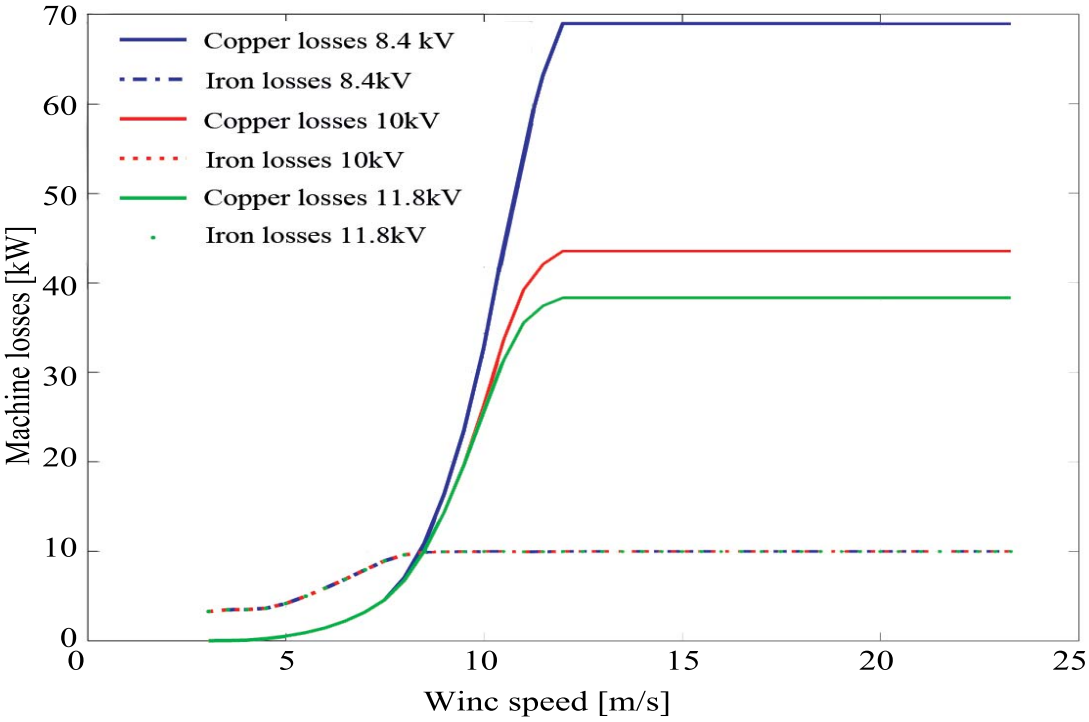

Fig. 4.27 Machine losses for different wind speed and different DC link, IGBT-converter

4.4 Equilibrium DC voltage and losses

For each wind speed as well as each case setup, there is a specific P-V_d curve which shows the power can be extracted from the wind energy. For each curve and the desired power, there are two equilibrium DC voltages, as can be seen in Fig. 4.28, for Series compensation scenario at rated wind speed with 5MW output power. The illustrated figure is obtained form (4-14).

As was explained, No compensation cannot give the rated power of the PMSG, the solid red curve. For the other cases in Fig. 4.28, there are two choices for selection of the DC voltages; for example for P4, the blue dashed curve, 5MW power can be achieved at 1600V as well as 5900V DC voltages.

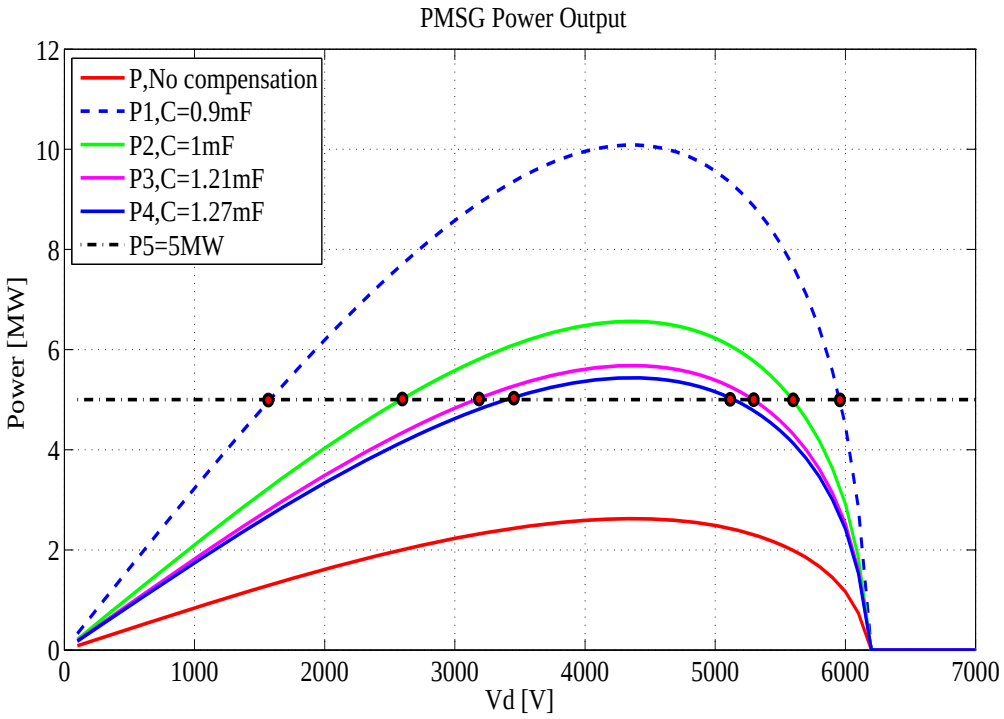

Fig. 4.28 Different DC voltage for 5MW output power, series compensation model

To explain that how the selection of DC voltages is important, the total machine losses (Fig. 4.26) should be redrawn for different DC voltages. Fig. 4.29 shows the that the series compensation with higher DC voltage has less power losses.

The solid blue curve, in Fig. 4.29, has the lower DC link voltage and higher power losses. For this curve, the DC voltage increases from 45V to 3700V when the wind speed rises from 4[m/s] to 12[m/s]. The DC voltage remains constant for the wind speed higher than 12[m/s].

Nevertheless, the solid red curve shows the machine power losses for the higher DC link voltage. The DC voltage is 4005[V] for the 4 [m/s] wind speed and it reaches to 6300[V] at 8[m/s] wind speed then for the rated operation at 12[m/s] wind speed the DC voltage changes to 5650[V]. The result clarifies that with higher DC voltage it becomes possible to have less power losses due to the reduction of the stator current by increasing the voltage and this matter applies to all three cases, as will be shown in Section 4.5.

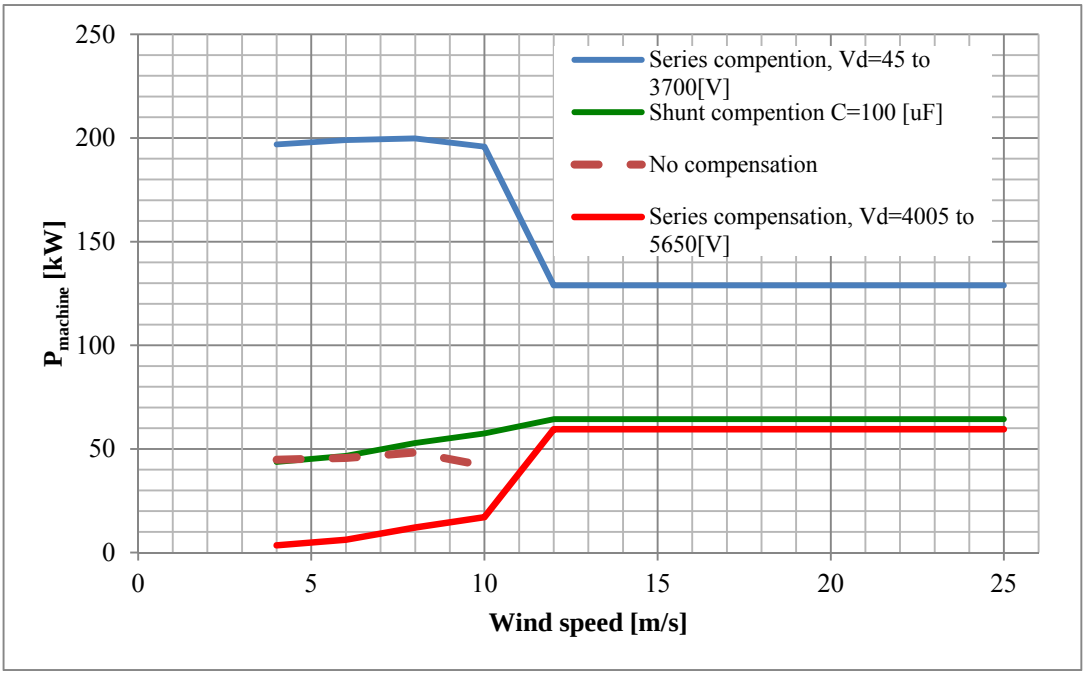

Fig. 4.29 Total machine losses for different DC voltages

Table 4-6 The effect of DC link voltage on the current and reactive power, series compensation

	Low voltage		High voltage		Low voltage		High voltage		Low voltage		High voltage	
Load	100%	5%	100%	5%	100%	5%	100%	5%	100%	5%	100%	5%
C	0.000890785				0.001080832				0.001209897			
Xc	3.6	5.9	3.6	5.9	2.9	4.9	2.9	4.9	2.6	4.4	2.6	4.4
Ia RMS	2000	2300	679	55	1368	1538	713	51	1068	1179	759	54
Vdc	1700	90	5700	4055	2700	125	5300	4030	3500	1560	4900	4025
Q[MVar]	14.3	31.3	1.65	0.02	5.51	11.5	1.50	0.01	3.00	10.6	1.52	0.01
P	5	0.25	5	0.25	5	0.25	5	0.25	5	0.25	5	0.25
Wind speed [m/s]	12	4.5	12	4.5	12	4.5	12	4.5	12	4.5	12	4.5
Rotor speed RPM	750	453	750	453	750	453	750	453	750	453	750	453

The results of simulation for different equilibrium DC voltages and different series capacitances are reported in Table 4-6 which shows the required reactive power for various operation points as well as RMS currents. As can be seen, for none of the cases, working on the low voltage side is a good choice; not only are the currents too high, the required reactive powers are also considerably big. Therefore, the operation points should be selected from the high voltage columns. Considering the resonance band as well as low RMS current, the DC voltage of 5300[V] for full load operation and 4030[V] for 5% of load can be good choices.

The same scenario happens for the shunt compensation and the shunt compensation has the high DC link voltages and high required reactive power in comparison with the series compensation, as presented in Table 4-7.

Table 4-7 The effect of DC link voltage on the current and reactive power, shunt compensation

	Low voltage		High voltage		Low voltage		High voltage	
Load	100%	5%	100%	5%	100%	5%	100%	5%
C	0.000106				0.00009			
Xc	30	50	30	50	35	59	35	59
Ia RMS	715	600	681	147	677	604	588	125
Vdc	6600	320	12500	5022	6840	310	10000	4850
Q[MVar]	1.451	0.002	5.203	0.507	1.323	0.002	2.827	0.402
P	5	0.25	5	0.25	5	0.25	5	0.25
Wind speed [m/s]	12	4.5	12	4.5	12	4.5	12	4.5
Rotor speed RPM	750	453	750	453	750	453	750	453

A worthy operation point for shunt compensation can be C=90[uF] with High voltage column, due to reasonable current, DC voltage and reactive power. However, it is noticeable that the maximum required reactive power in the shunt compensation case (2.8MVar) is higher for the than series compensation case (1.5MVar).

4.5 Diode rectifier vs. active rectifier

In this chapter the two main scenarios have been compared. Scenario one is the PMSG connected to the diode rectifier which includes 3 approaches, No compensation, Series compensation, and Shunt compensation. Scenario two is the PMGS converter connected to the IGBT-converter for DC link voltage of 10 [kV]. This DC voltage has been chosen since this is the suitable DC-link voltage for the system with active rectifier and it has both lower on-state and switching losses in the IGBTs [12]. For the series compensation at rated operation (V_d=5650[V]) and at 6[m/s] wind speed (V_d=5080[V]) the currents flowing in a diode module are depicted in Fig. 4.30.

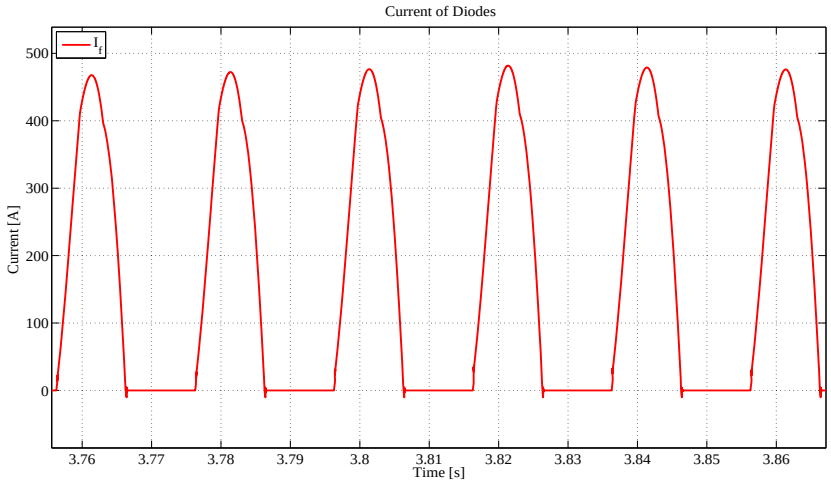

a) Conduction current of a diode at full load

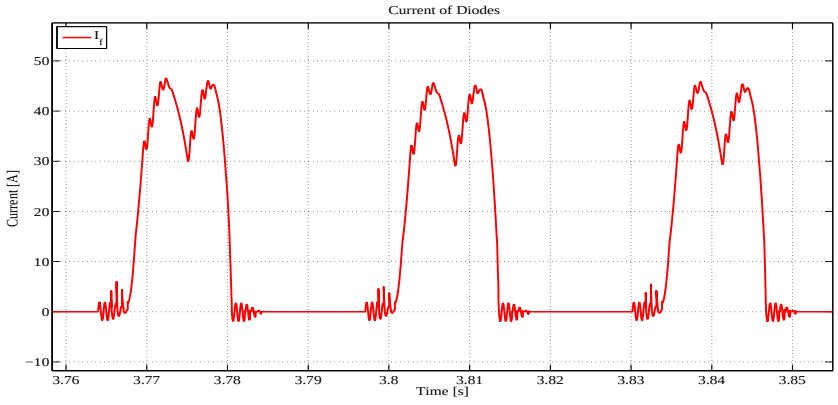

b) Conduction current of a diode at 5% of load

Fig. 4.30 Conduction current of one diode module

The total power loss of the diode rectifier is the average value of the instantaneous power of 24 diode modules. Then, according to (4-17), conduction losses of the diode rectifier can be calculated.

Fig. 4.31 depicts the instantaneous power losses in one diode for the series compensation at full and 5% of load operation.

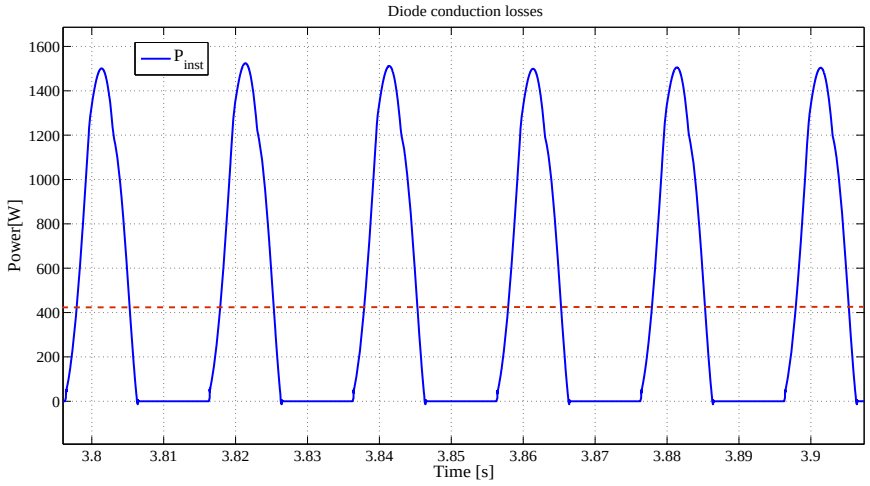

a) Instantaneous and average power for one diode at full load

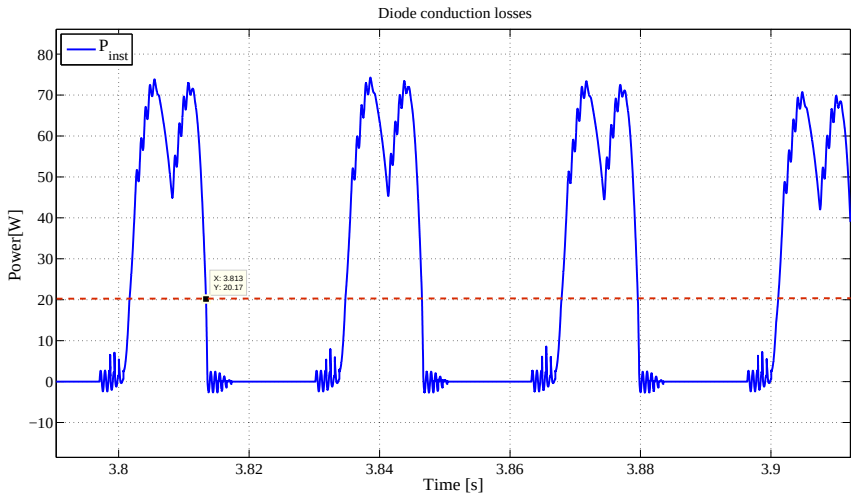

b) Instantaneous and average power for one diode at 5% of load

Fig. 4.31 Diode conduction losses

It can be seen in Fig. 4.32 that the losses of the IGBT-converter are much higher than the diode rectifier. The most dominant losses belong to the switching losses. It should be noted that all losses have been reduced for the diode rectifier cases by using the higher equilibrium voltages.

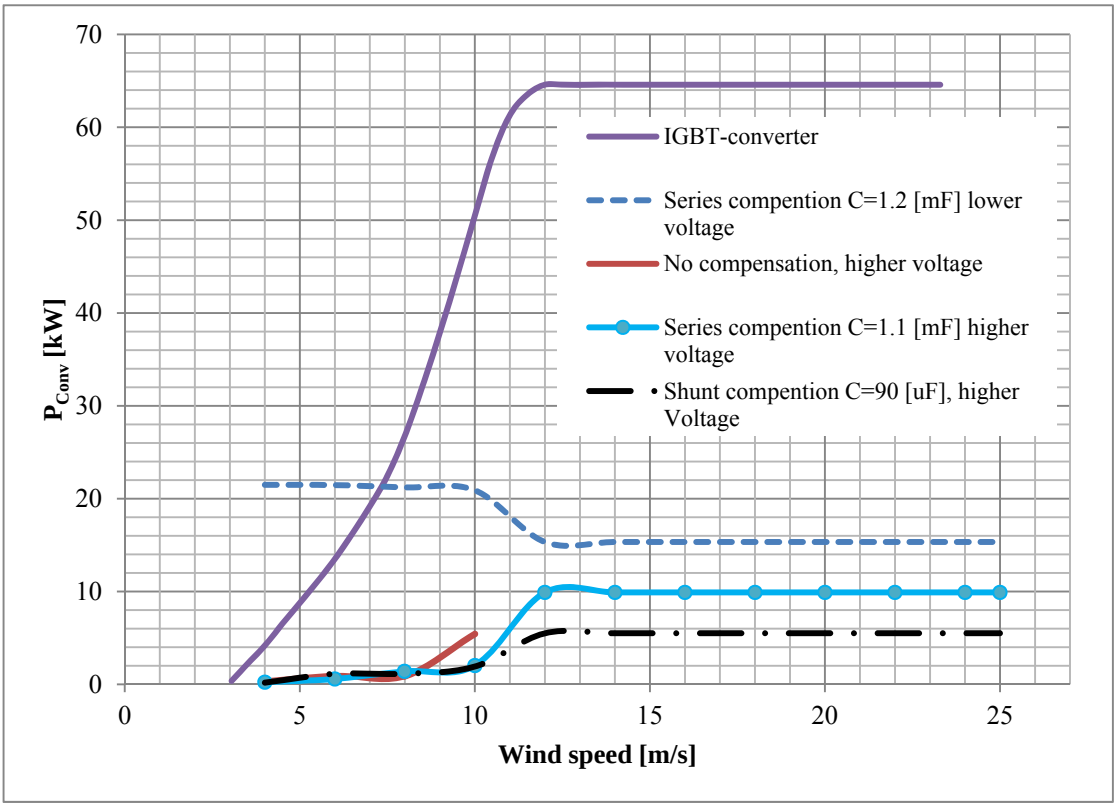

Fig. 4.32 Diode rectifier losses and IGBT-converter losses

As can be seen in Fig. 4.33, the diode rectifier and the IGBT-converter have an influence on the machine losses. The diode rectifier with series compensation causes higher losses in the machine; since the stator current is higher with series compensation. 90[uF] capacitance is selected for the shunt compensation and for each equilibrium point the higher DC voltage is set for the DC link voltage. The results show that the shunt compensation has the lowest total machine losses at rated operation. However, for the wind speed lower than 11[m/s], the series compensation case has the lowest total machine losses. At low wind speed the current frequency is low; accordingly, the shunt reactance is lower than for the rated operation. Subsequently, for the shunt compensation case the angle between voltage and current is about -80°degree which causes higher power losses for low wind speeds.

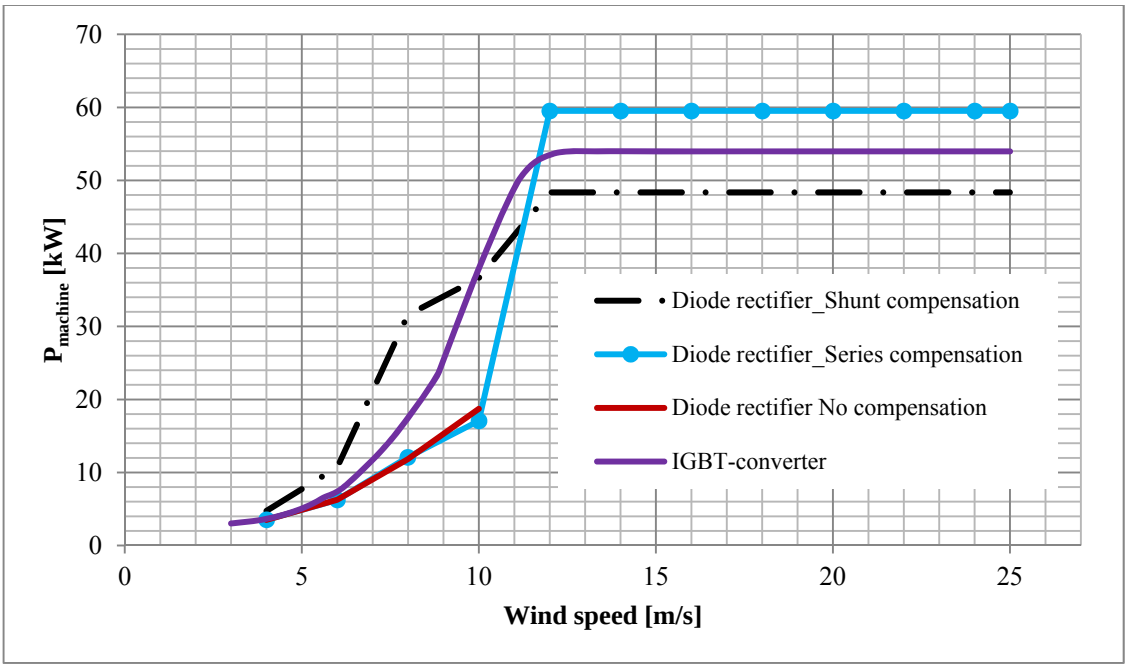

Fig. 4.33 The impact of IGBT-converter and diode rectifier on the machine losses, for the series compensation V_d=5650[V], for the shunt compensation V_d=10[kV] at the rated wind speed

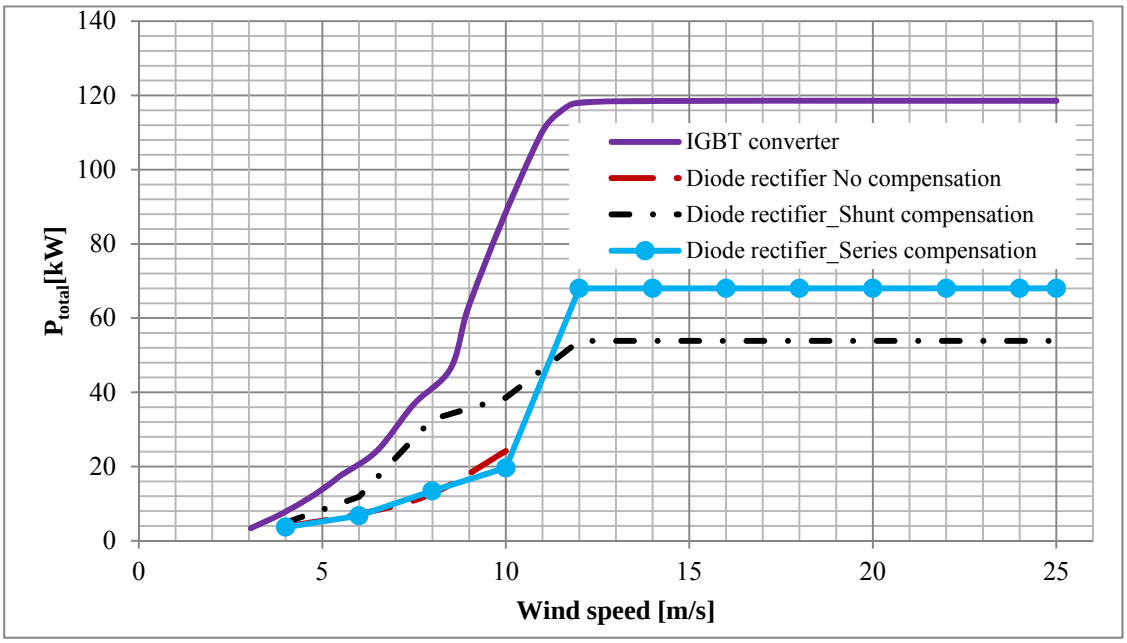

Fig. 4.34 Total losses for the diode rectifier with C=90[uF] for shunt compensation, C=1.1[mF] for series compensation, and IGBT converter with V_d= 10 [kV]

The total losses which are the summation of losses in the machine and the rectification methods are presented in Fig. 4.34. As can be seen the diode rectifier with series compensation has the lowest power dissipation for the wind speed lower than 11[m/s] and at full load operation the shunt compensation has the lowest losses.

Nevertheless, the IGBT-converter has lower machine losses for the wind speed higher than 12 [m/s], because of the controlling the stator current, the growth of IGBT-converter losses severely increases the total losses at the rated operation.

The efficiencies of different scenarios as a function of wind speed are depicted in Fig. 4.35. As was expected from total losses figure, the series compensation case is more efficient for wind speed lower than 11[m/s] and the shunt compensation model has a better efficiency for wind speed higher than 12[m/s].

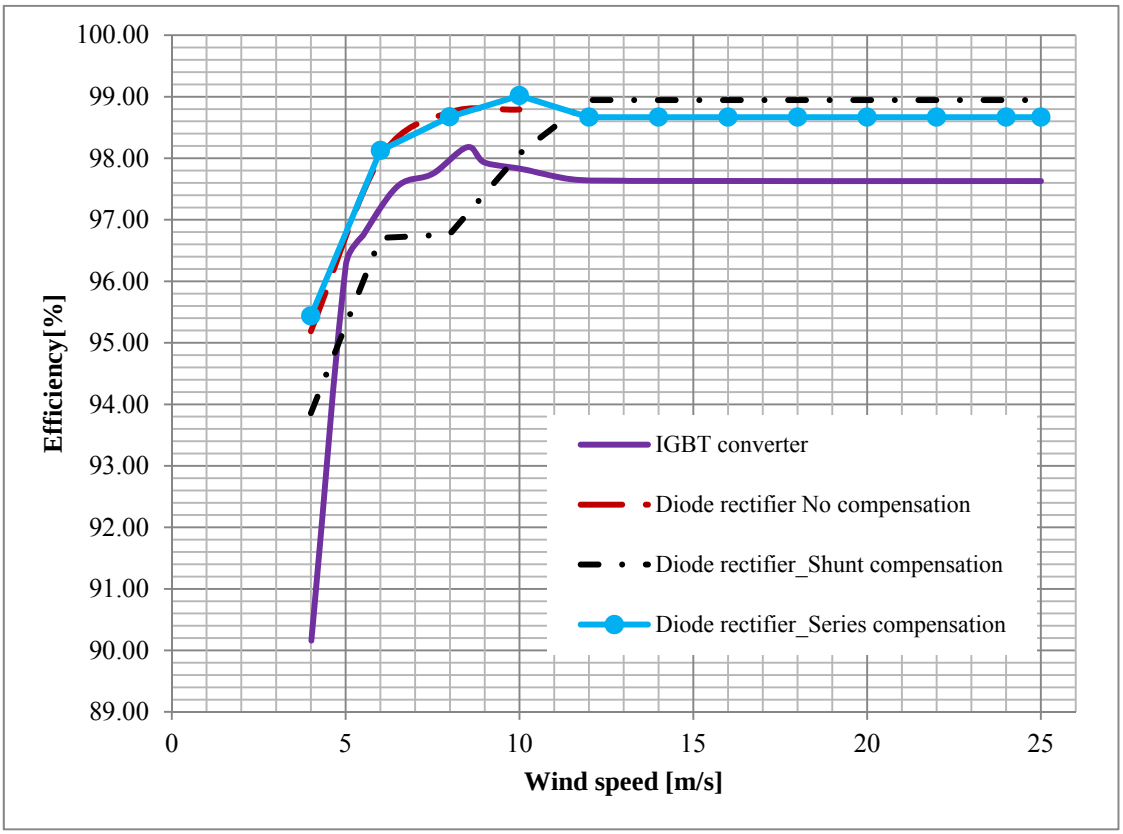

Fig. 4.35 Efficiency variations with wind speed

The efficiency and losses of the series compensation, the shunt compensation and the IGBT-converter for full load operation as well as 5% of load are presented in Table 4-8.

Table 4-8 Efficiency and losses of the diode rectifier vs. active rectifier

	Total power losses	loss%	Efficiency at 5% of load	Efficiency at 100% of load
Series compensation	68015	1.36	97.3	98.64
Shunt compensation	53846	1.08	95.25	98.92
IGBT converter	118047	2.36	92.97	97.63

Chapter 5

5. Conclusions

5.1 Results from present work

In this thesis work, it is shown and thoroughly explained how it is possible to use a diode rectifier for an investigated 5 MW permanent magnet synchronous generating system for a wind turbine to be connected to an HVDC collection grid. The system simulation has been carried out in SimPowerSystems. As it can be seen in Chapter 3, the PMGS dynamic model matches the investigated machine. The simulated system in SimPowerSystems and Simplorer verifies that the design of diode rectifier with full bridge converter is a good option for wind applications.

An analytical method for calculating the relation between electrical power and the voltage of the DC-link has been proposed in Chapter 4. The theoretical analysis has been confirmed by simulation results. The proposed method allows finding a suitable DC-link voltage to extract the available maximum power of the generator.

In order to obtain the desired electrical power, with a diode rectifier, reactive power compensation is needed. The result found was that series compensation can be the best chose to get the full rated power of the generator and also have low total losses.

The shunt compensation scenario requires higher reactive power (2.8MVar) in comparison with the series compensation scenario for the same output power (5MW).

Two compensating methods, series compensation and shunt compensation, to extract the full rated power of the generator have been simulated and compared with the IGBT-converter scenario.

The effect of equilibrium DC voltage on the system has been investigated and the result verifies that the higher DC voltage decreases the losses in machine and the rectifier, as well as reducing the required reactive power.

The advantages and disadvantages of a diode rectifier and an active rectifier have been discussed, and a conclusion is that the losses in both rectifiers are considerable.

The total losses with the diode rectifier with series compensation as well as shunt compensation are 1.36% and 1.08% while the total losses with the active rectifier (IGBT-converter) is 2.36% at rated wind speed (12 [m/s]).

The series compensation method has better efficiency (99.86%) at low wind speed and the shunt compensation method has better efficiency (98.93%) at high wind speed.

5.2 Future work

The main focus of the thesis has been on the behaviour of the system, the voltage and the current wave forms, and the comparison of different configurations. The verification of the PMSG model in SimPowerSystem with Simplorer and analytical model has been fulfilled. It can be of interest to expand the work by assigning some filters and connecting the diode rectifier to a DC/DC converter.

In order to have more full-covering result of the efficiency of the system, it could be interesting to investigate the losses in the cables and thermal losses in the rectifier.

It is also possible to study the best combination of series and shunt compensation for such a system.

In this work, it is assumed that the temperature is always 20℃, for further investigation the effect of temperature rise, the need of cooling system and the impact of temperature on the efficiency can be of interest.

The annual energy losses can be integrated and the result will be useful to show the annual energy yield of the system.

In this project, it is assumed the wind speed is constant for each operation point. Hence, the future work can be done with the consideration of variation of wind speed as well as a design of a control system for current and torque control.

Finally, a cost study of the system can be evaluated and the result can be compared with an IGBT-converter scenario and EMSG (Electrically Magnetized Synchronous Generator).

References

[1] "Oceanweather," [Online]. Available: http://www.oceanweather.com/data/. [Accessed 20 July 2012].

[2] S. G. COLINO, DC High Voltage Connection Systems for Offshore Wind Turbines, Göteborg, 2010.

[3] ENERCON, "ENERCON," [Online]. Available: http://www.enercon.de/en-en/753.htm. [Accessed 29 3 2012].

[4] MathWork, "MathWork," [Online]. Available:http://www.mathworks.se/help/toolbox/physmod/powersys/ref/igbt.html. [Accessed 23 March 2012].

[5] O. Carlson, "Sustainable Power Production and Transportation," Gothenburg, Chalmers University of Technology, 2011,09,01, p. 14.

[6] N. Mohan, T. M. Undeland and W. P. Robbins, Power Electronics Converters, Applications, and Design.

[7] "ABB i Sverige," ABB, [Online]. Available: http://www.abb.se/product/db0003db004291/c12573e7003304adc1256b820064c335.aspx. [Accessed 05 04 2012].

[8] L. Max, Energy Evaluation for DC/DC Converters in DC-Based Wind Farms, Göteborg: CHALMERS UNIVERSITY OF TECHNOLOGY, 2007.

[9] M. S. Chinthavali, L. M. Tolbert and B. Ozpineci, "4H-SiC GTO thyristor and p-n diode loss models for HVDC converter," *IEEE IAC 04,* vol. 2, pp. 128-1243, 2004.

[10] D. T. Morisette and J. A. Cooper, "Theoretical Comparison of SiC PiN and Schottky Diodes Based on Power Dissipation Considerations," *IEEE Transactions on Electron Devices,* vol. 49, no. 9, pp. 1657-1664, 2002.

[11] Semikron, "Theory of Loss and Temperature Calculation," 2008. [Online]. Available: http://www.semikron.com/skcompub/en/eng_3_2_1_3.pdf.

[12] P. Roshanfekr, T. Thiringer and S. Lundmark, "Efficiency comparison of a 5 MW wind turbine PMSG-equipped generating system using various dc-link voltages," in *EVER*, Monaco, 2012.

[13] T. Thiringer, J. Paixao and M. Bongiorno, "Monintoring of the ride-through ability of a 2MW wind trubine in Tvååker, Halland," Chalmers University of Technology, 2009.

[14] ANSYS, "ANSYS," 15 3 2012. [Online]. Available: http://www.ansys.com/Products Simulation+Technology/Electromagnetics/Electromechanical+Design/ANSYS+Simp lorer.

[15] F. Sulla, "Fault Behavior of Wind Turbines," Lund University, Lund, 2012.

[16] ABB HiPak and IGBT Module, "5SNA 0750G650300," in *Datasheet*, ABB Switzerland Ltd, 2009.

Appendix

Machine Data

PERMANENT MAGNET SYNCHRONOUS GENERATOR DESIGN

GENERAL DATA

Rated Output Power (kW):	5000
Rated Voltage (V):	4800
Number of Poles:	8
Frequency (Hz):	50
Frictional Loss (W):	0
Windage Loss (W):	0
Rotor Position:	Inner
Operating Temperature (C):	75

STATOR DATA

Number of Stator Slots:	24
Outer Diameter of Stator (mm):	1100
Inner Diameter of Stator (mm):	757.9
Top Tooth Width (mm):	59.9173
Bottom Tooth Width (mm):	53.6687
Skew Width (Number of Slots):	0

Length of Stator Core (mm):	945
Stacking Factor of Stator Core:	0.95
Number of Parallel Branches:	2
Number of Conductors per Slot:	44
Average Coil Pitch:	2
Number of Wires per Conductor:	1
Wire Diameter (mm):	9.266
Slot Area (mm^2):	6759.14
Net Slot Area (mm^2):	6190.79
Stator Slot Fill Factor (%):	61.0227
Coil Half-Turn Length (mm):	1323.43

ROTOR DATA

Minimum Air Gap (mm):	3
Inner Diameter (mm):	400.4
Length of Rotor (mm):	945
Stacking Factor of Iron Core:	0.95
Polar Arc Radius (mm):	195.95
Mechanical Pole Embrace:	0.7
Electrical Pole Embrace:	0.596409
Max. Thickness of Magnet (mm):	28
Width of Magnet (mm):	197.067

Type of Magnet:	NdFe30
Magnetic Shaft:	No

PERMANENT MAGNET DATA

Residual Flux Density (Tesla):	1.1
Coercive Force (kA/m): 838	
Maximum Energy Density (kJ/m^3):	230.45
Relative Recoil Permeability:	1.0446
Demagnetized Flux Density (Tesla):	0.647015
Recoil Residual Flux Density (Tesla):	1.1
Recoil Coercive Force (kA/m):	838

MATERIAL CONSUMPTION

Armature Copper Density (kg/m^3):	8900
Permanent Magnet Density (kg/m^3):	7550
Armature Core Steel Density (kg/m^3):	7700
Rotor Core Steel Density (kg/m^3):	7700
Armature Copper Weight (kg):	838.741
Permanent Magnet Weight (kg):	271.133
Armature Core Steel Weight (kg):	2329.36
Rotor Core Steel Weight (kg):	1758.83
Total Net Weight (kg):	5198.06

Armature Core Steel Consumption (kg):	8410.02
Rotor Core Steel Consumption (kg):	3376.57

STEADY STATE PARAMETERS

Stator Winding Factor:	0.866025
D-Axis Reactive Reactance Xad (ohm):	2.92968
Q-Axis Reactive Reactance Xaq (ohm):	2.92968
D-Axis Reactance X1+Xad (ohm):	4.83054
Q-Axis Reactance X1+Xaq (ohm):	4.83054
Armature Leakage Reactance X1 (ohm):	1.90086
Zero-Sequence Reactance X0 (ohm):	0.394111
Armature Phase Resistance R1 (ohm):	0.0374772
Armature Phase Resistance at 20C (ohm):	0.030828

NO-LOAD MAGNETIC DATA

Stator-Teeth Flux Density (Tesla):	1.78945
Stator-Yoke Flux Density (Tesla):	1.64989
Rotor-Yoke Flux Density (Tesla):	0.614729
Air-Gap Flux Density (Tesla):	0.966052
Magnet Flux Density (Tesla):	0.87569
Fundamental Induced RMS Line Voltage (V):	5032.09
THD of Induced Voltage (%):	11.0593

Cogging Torque (N.m):	177.89

FULL-LOAD DATA

RMS Line Current (A):	742.962
RMS Phase Current (A):	742.962
RMS Phase Voltage (V):	2771.18
Armature Thermal Load (A^2/mm^3):	90.7613
Specific Electric Loading (A/mm):	16.4755
Armature Current Density (A/mm^2):	5.50886
Frictional and Windage Loss (W):	0
Iron-Core Loss (W):	9883.42
Armature Copper Loss (W):	62061.4
Total Loss (W):	71944.8
Output Power (W):	5.00152e+006
Input Power (W):	5.07346e+006
Efficiency (%):	98.5819
Apparent Power (VA):	6.17663e+006
Power Factor:	0.809748
Synchronous Speed (rpm):	750
Rated Torque (N.m):	64597.3
Power Angle (degree):	70.0171
Maximum Output Power (W):	5.31863e+006

Short Circuit Current (A):	641.93

TRANSIENT FEA INPUT DATA

For Armature Winding:	
Number of Turns:	176
Parallel Branches:	2
Terminal Resistance (ohm):	0.0374772
End Leakage Inductance (H):	0.000393811
2D Equivalent Value:	
Equivalent Model Depth (mm):	945
Equivalent Stator Stacking Factor:	0.95
Equivalent Rotor Stacking Factor:	0.95
Equivalent Br (Tesla):	1.1
Equivalent Hc (kA/m):	838
Estimated Rotor Inertia (kg m^2):	231.295

V_{RRM} = 6500 V
I_F = 2x 600 A

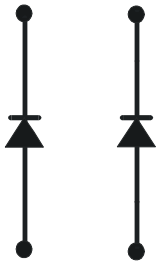

ABB HiPak™

DIODE Module

5SLD 0600J650100

Doc. No. 5SYA 1412-00 Aug. 10

- **Low-loss, rugged SPT diode**
- **Smooth switching SPT diode for good EMC**
- **Industry standard package**
- **High power density**
- **AlSiC base-plate for high power cycling capability**
- **AlN substrate for low thermal resistance**

Maximum rated values [1)]

Parameter	Symbol	Conditions	min	max	Unit
Repetitive peak reverse voltage	V_{RRM}			6500	V
DC forward current	I_F			600	A
Peak forward current	I_{FRM}	t_p = 1ms		1200	A
Total power dissipation	P_{tot}	T_c = 25 °C, per diode		4760	W
Surge current	I_{FSM}	V_R = 0 V, T_{vj} = 125 °C, t_p = 10 ms, half-sinewave		6000	A
Isolation voltage	V_{isol}	1 min, f = 50 Hz		10200	V
Junction temperature	T_{vj}			125	°C
Junction operating temperature	$T_{vj(op)}$		-40	125	°C
Case temperature	T_c		-40	125	°C
Storage temperature	T_{stg}		-40	125	°C

[1)] Maximum rated values indicate limits beyond which damage to the device may occur per IEC 60747

Diode characteristic values [2]

Parameter	Symbol	Conditions		min	typ	max	Unit
Forward voltage [3]	V_F	I_F = 600 A	T_{vj} = 25 °C		3.2	3.8	V
			T_{vj} = 125 °C		3.4	4.0	
Continuous reverse current	I_R	V_R = 6500 V	T_{vj} = 25 °C			6	mA
			T_{vj} = 125 °C		35	75	
Reverse recovery current	I_{rr}	V_R = 3600 V, I_F = 600 A, V_{GE} = ±15 V, di/dt = 2500 A/µs L_σ = 280 nH inductive load, switch:	T_{vj} = 25 °C		790		A
			T_{vj} = 125 °C		990		
Recovered charge	Q_{rr}		T_{vj} = 25 °C		700		µC
			T_{vj} = 125 °C		1200		
Reverse recovery time	t_{rr}		T_{vj} = 25 °C		1700		ns
			T_{vj} = 125 °C		2200		
Reverse recovery energy	E_{rec}		T_{vj} = 25 °C		1100		mJ
			T_{vj} = 125 °C		2200		
Module stray inductance	$L_{\sigma AC}$	per diode			36		nH
Resistance, terminal-chip	$R_{AA'+CC'}$	per diode	T_C = 25 °C		0.2		mΩ
			T_C = 125 °C		0.3		

[2] Characteristic values according to IEC 60747 – 2
[3] Forward voltage is given at chip level

Thermal properties [4]

Parameter	Symbol	Conditions	min	typ	max	Unit
Diode thermal resistance junction to case	$R_{th(j-c)DIODE}$				0.021	K/W
Diode thermal resistance case to heatsink [5]	$R_{th(c-s)DIODE}$	diode per switch, λ grease = 1W/m x K		0.018		K/W

Mechanical properties [4]

Parameter	Symbol	Conditions		min	typ	max	Unit
Dimensions	L x W x H	Typical , see outline drawing		130 x 140 x 48			mm
Clearance distance in air	d_a	according to IEC 60664-1 and EN 50124-1	Term. to base:	40			mm
			Term. to term:	26			
Surface creepage distance	d_s	according to IEC 60664-1 and EN 50124-1	Term. to base:	64			mm
			Term. to term:	56			
Comparative tracking index	CTI			≥ 600			
Mounting torques [5]	M_s	Base-heatsink, M6 screws		4		6	Nm
	M_{t1}	Main terminals, M8 screws		8		10	
Mass	m				1150		g

[4] Thermal and mechanical properties according to IEC 60747 – 15
[5] For detailed mounting instructions refer to ABB document no. 5SYA 2039 - 01

Electrical configuration

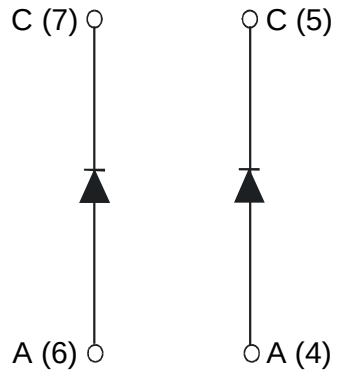

Outline drawing [5]

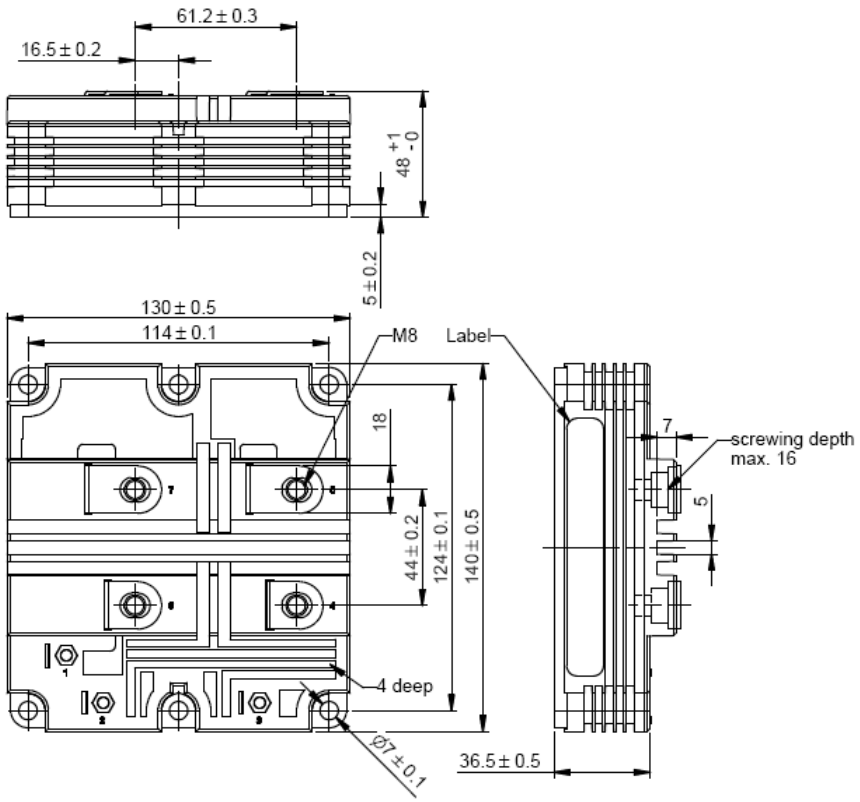

Note: all dimensions are shown in mm

[5] For detailed mounting instructions refer to ABB document no. 5SYA 2039 - 01

This is an electrostatic sensitive device, please observe the international standard IEC 60747-1, chap. IX.
This product has been designed and qualified for industrial level.

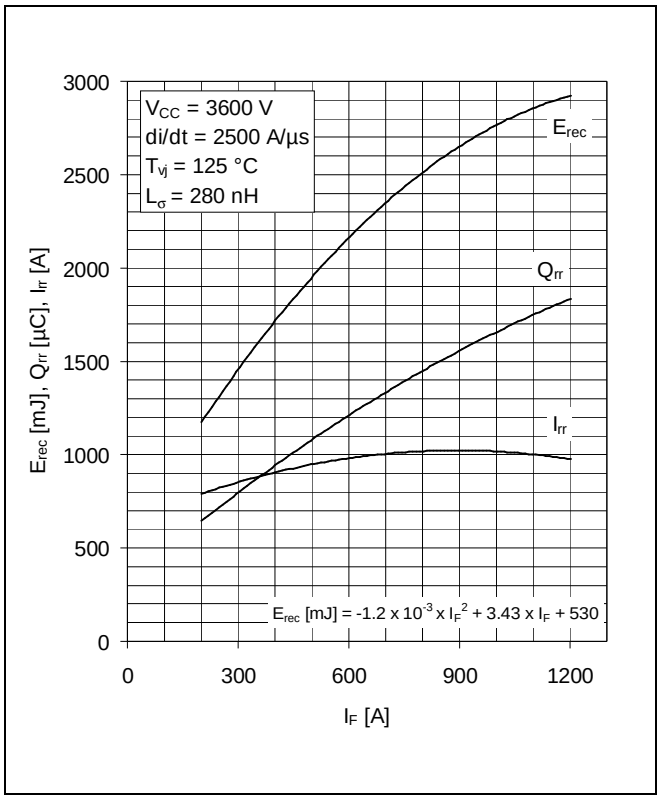

Fig. 1 Typical reverse recovery characteristics vs forward current

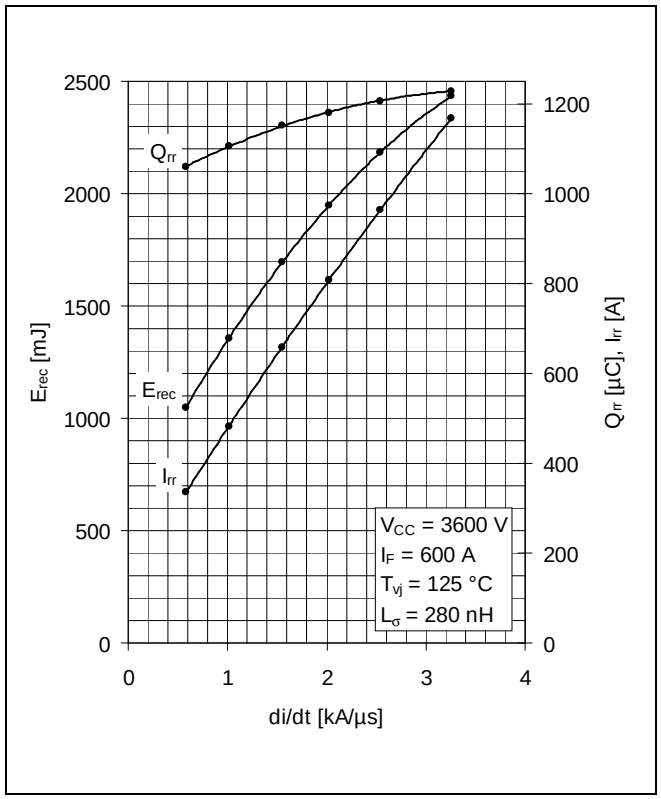

Fig. 2 Typical reverse recovery characteristics vs di/dt

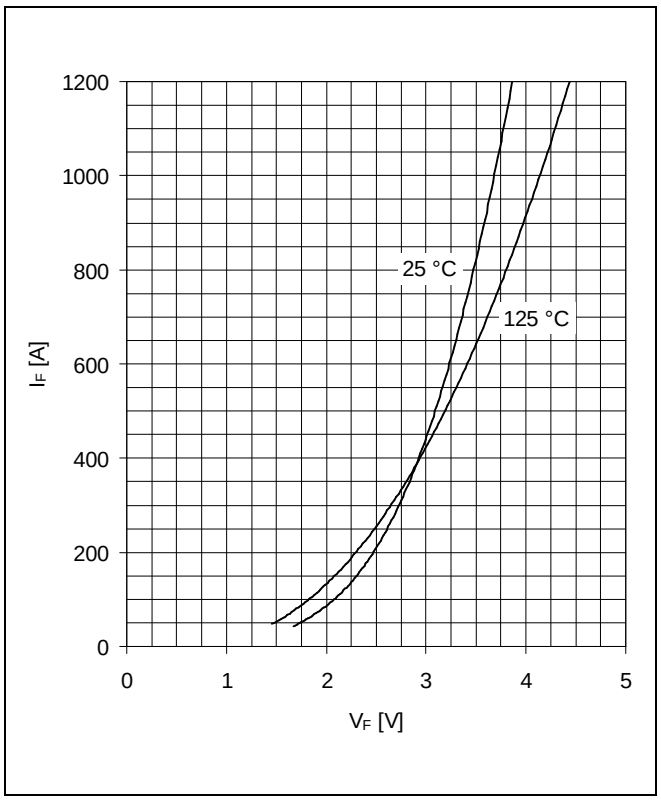

Fig. 3 Typical diode forward characteristics, chip level

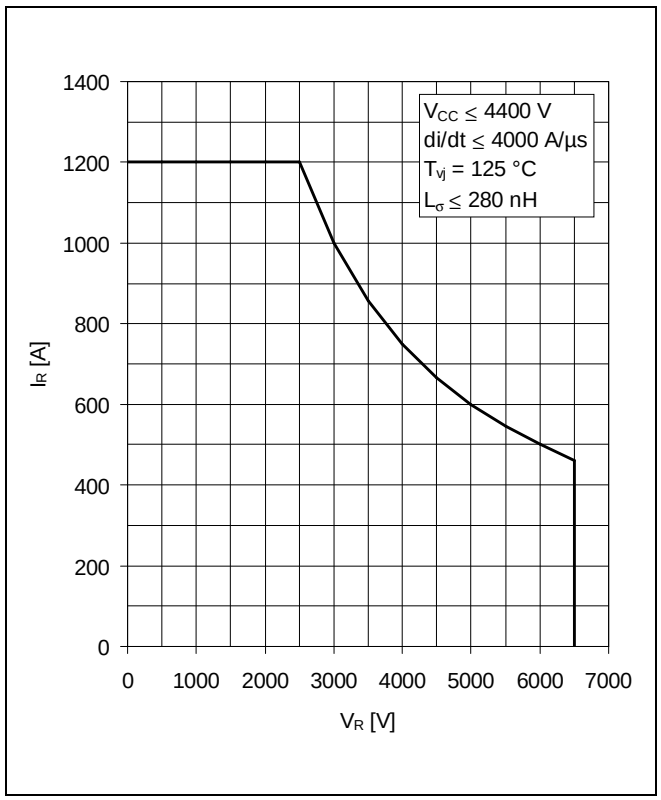

Fig. 4 Safe operating area diode (SOA)

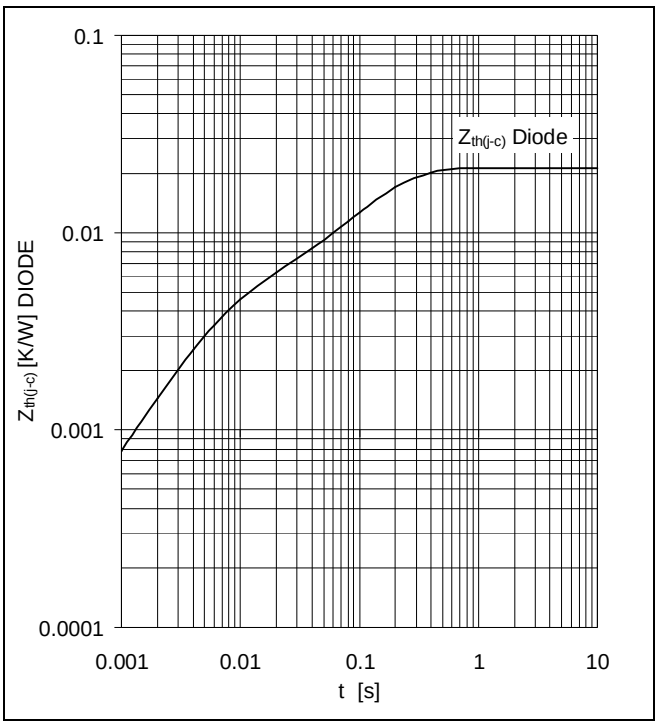

Fig. 5 Thermal impedance vs time

Analytical function for transient thermal impedance:

$$Z_{th\,(j\text{-}c)}(t) = \sum_{i=1}^{n} R_i\,(1 - e^{-t/t_i})$$

DIODE

i	1	2	3	4	5
R_i(K/kW)	17	4.2			
τ_i(ms)	144	5.83			

For detailed information refer to:

- 5SYA 2042 Failure rates of HiPak modules due to cosmic rays
- 5SYA 2043 Load – cycle capability of HiPaks
- 5SYA 2045 Thermal runaway during blocking
- 5SYA 2058 Surge currents for IGBT diodes
- 5SZK 9120 Specification of environmental class for HiPak

ABB Switzerland Ltd
Semiconductors
Fabrikstrasse 3
CH-5600 Lenzburg, Switzerland

Telephone +41 (0)58 586 1419
Fax +41 (0)58 586 1306
Email abbsem@ch.abb.com
Internet www.abb.com/semiconductors

Doc. No. 5SYA 1412-00 Aug. 10